Escola Politècnica Superior
d'Enginyeria de Vilanova i la Geltrú
UNIVERSITAT POLITÈCNICA DE CATALUNYA

FINAL DEGREE PROJECT

TÍTOL: **STUDY OF DIFFERENT AERODYNAMICS MODIFICATIONS FOR SMALL AXIAL FLOW FAN**

AUTORS: BIN ABDUL JALIL, ANAS

DATA DE PRESENTACIÓ: Julio, 2017

RESUM

En este proyecto, se investigaron los efectos de los álabes en el comportamiento aerodinámico de pequeños ventiladores axiales para disminuir la turbulencia del flujo en su superficie y generalmente para mejorar el rendimiento aerodinámico. Se estudiaron mediante simulación dos modificaciones en la superficie de los alabes de un pequeño ventilador axial (modelo 1, prototipo): la situación de un “winglet” en el extremo del álabe (modelo 2) y el diseño denominado de “aleta de tiburón” (modelo 3), para conocer cómo las modificaciones afectan a su comportamiento aerodinámico. Se modeló en 3D el ventilador prototipo, así como el ventilador con sus modificaciones, y se realizaron las simulaciones numéricas en estado estacionario mediante el software comercial NX Siemens PLM versión 10 (simulación avanzada NX CAE). Las ecuaciones N-S con el análisis de elementos finitos estándar y el modelo de turbulencia k-ε fueron adoptados para llevar a cabo el cálculo de la simulación. La comparación entre los resultados experimentales y simulación numérica se realizó en vistas a validar la simulación del prototipo. Se analizaron el efecto del winglet y del diseño de aleta de tiburón, concluyendo que el método de añadir un winglet al alabe del prototipo tienen influencia en la reducción de la vorticidad en la punta del alabe, como consecuencia de la disminución de la diferencia de presiones a ambos lados del extremo del álabe. Los resultados muestran también que la adición del diseño de aletas de tiburón en la superficie de succión puede canalizar la turbulencia en el borde posterior del alabe.

Paraules clau (màxim 10):

Ventilador	Axial	Alabes	Modificaciones
Siemens NX10	Flujo	CFD	

ABSTRACT

In this project, the effects of airfoils on the aerodynamic performance of small axial fans were investigated to improve airflow turbulence on the blade surface and generally to improve the aerodynamic performance. Two modifications were made on the blades surface to know why and how the modifications affect the aerodynamic performance. The 3D steady numerical simulation for all models done by using CFD commercial software NX Siemens PLM version 10 (advanced simulation NX CAE). The N-S equations with finite element analysis and the standard k-ε turbulence model were adopted to carry out the steady simulation calculation. A comparison between experimental results and numerical simulation also have been carried out to see how the modifications affect the aerodynamic performance and static characteristics of the fan. The effect of the winglet and shark-fin blade designs were analysed. It is concluded that the method of adding winglet to the prototype blade has an influence on reducing vorticity at the tip of the blade. The results show that by adding shark fin blade on the suction surface of the blade can channel the turbulence at the trailing edge of the blade.

Keywords (10 maximum):

Fan	Axial	Blades	Modifications
Siemens NX10	Flow	CFD	

INDEX

1. Introduction 11
2. Objective 12
3. Literature view 13
3.1 Fan Classification 13
3.2 Velocity diagrams 14
3.3 Euler equation for axial-flow fans 15
3.4 Three-dimensional flow effects: radial equilibrium requirement 16
3.5 Contraction coefficient 18
3.6 Mass flow coefficient 18
3.7 Static pressure coefficient 18
4. Study of fan 19
4.1 General data 19
4.2 Theoretical study 19
4.2.1 Velocity diagrams 20
4.2.2 Pressure distribution 22
4.2.3 Contraction coefficient 23
4.2.4 Mass flow coefficient 23
4.2.5 Static pressure coefficient 24
4.3 Experimental measurements 24
4.3.1 Rotational velocity 24
4.3.2 Static pressure 25
4.3.3 Velocity 27
5. Study of modifications 28
5.1 Modification 1 28
5.2 Modification 2 29
6. Modeling and Simulation processes 30
6.1. Modelling process 30
6.1.1 Modelling of the three-dimensional solid hub 30
6.1.2 Modelling of the two-dimensional and three-dimensional blade profile 31
6.1.3 Modelling of the three-dimensional frame of a cooling fan 32
8.1.4 Assembling of the complete model of a cooling fan 33
6.2 Simulation 34
6.2.1 Governing equations 34
6.2.2 Computational domain 35
6.2.3 Mesh 35
6.2.4 Initial conditions 37
6.2.5 Boundary conditions 37
6.2.6 Solving methods of the steady calculation 38
6.2.7 Comparison of the experimental and numerical results of the axial fan 39

6.3 Modification 41
6.3.1 Mechanism analysis of the modified models 42
7. Conclusion 51
8. Recommendations 52
9. Acknowledgement 53
10. References 54

LIST OF FIGURES

Figure 3.1. Velocity diagrams at the inlet and outlet 14
Figure 3.2. Radial equilibrium requirement 16
Figure 4.1. Prototype pictures 19
Figure 4.2. Velocity diagram of inlet and outlet at hub. 20
Figure 4.3. Velocity diagram of inlet and outlet at midspan. 21
Figure 4.4. Velocity diagram of inlet and outlet at tip. 21
Figure 4.5. Logarithm of the tangential component of absolute velocity with respect to logarithm of radius. 22
Figure 4.6. Distribution of pressure. 23
Figure 4.7. Graph of Ψ against φ. 24
Figure 4.8. Pictures of how fan speed is recorded. 24
Figure 4.9. The picture of axial fan on the polystyrene. 25
Figure 4.10. (a), (b) and (c) shows the pictures how the experiment was set up. 26
Figure 4.12. Points where the tachometer was placed during the measurement. 27
Figure 5.1. A Cooling fan with a winglet. 28
Figure 5.2. Blade of modified models. 29
Figure 5.3. Shark fin blade case fan. 29
Figure 6.1. Modelling of the three-dimensional solid hub. The diameter of the hub is 34.5mm. 30
Figure 6.2. Three-dimensional solid hub. 31
Figure 6.3. Side view of the impeller with 1 blade. 31
Figure 6.4. Top view of the 3D impeller. 32
Figure 6.5. Isometric view of the frame before hole is made. 32
Figure 6.6. Isometric view of the frame after the hole was made. 33
Figure 6.7. Isometric view of finished frame modelling. 33
Figure 6.8. Complete assembly of a cooling fan. 34
Figure 6.9 Computational domain. 35
Figure 6.10. Mesh. 36
Figure 6.11. Element sensitivity test result. 36
Figure 6.12. Boundary condition. 37
Figure. 6.13. Average velocity value at 5 cm from the axial fan. 39
Figure. 6.14. Average velocity value at 30 cm from the axial fan. 40
Figure. 6.15. Average velocity value at 5 cm from the axial fan at the inlet. 40
Figure 6.16. Graph of comparison between experimental and numerical results. 41
Figure 6.17. Model 1 (Prototype). 41
Figure 6.18. Model 2 (Winglet). 42
Figure 6.19. Model 3 (Shark fin blade). 42
Figure 6.20. Axial velocity contours of the meridional plane (X=0). 43
Figure 6.21. Axial velocity with arrows of the meridional plane (X=0). 44
Figure 6.22 Static pressure contours of meridional plane (X=0). 44
Figure 6.23. Detail of axial velocity contours of the meridional plane (X=0). 45
Figure 6.24. Static pressure contours of the meridional plane (X=0) of the fans. 46
Figure 6.25. Static pressure contour distribution of the blade suction surface and the pressure surface of the three models. 46
Figure 6.26. Vorticity contour distributions of the meridional plane (X=0) of the fans. 47
Figure 6.27. Three different axial cross-sections. 48
Figure 6.28. Diffuser effect. 49
Figure 6.29. Three different cross-sections of vorticity. 49

LIST OF TABLES

Table 4.1. Main parameters of the prototype fan. 19
Table 4.2. Main specifications of the prototype fan. 19
Table 4.3. Fan operation data. 20
Table 4.4. Inlet and outlet velocities (design conditions). 20
Table 4.5. Angle of various sections of blade. 20
Table 4.6. values of ln r and ln C_{2U}. 21
Table 4.7. Values of theoretical pressures. 22
Table 4.8. Values of coefficient of contraction. 23
Table 4.9. Values of flow coefficients. 23
Table 4.10. Values of pressure coefficients. 24
Table 4.11. Values of velocities, airflows and different of static pressure. 26
Table 4.12. Inlet velocities at the different points. 27
Table 4.13. Outlet velocities at different points. 27
Table 6.1. Element counts of different sections. 36
Table 6.2. Experimental and numerical results. 40

GLOSSARY

A	flow passage area normal (m^2)
C	corrected axial velocity (m/s)
c	absolute flow velocity (m/s)
D	diameter (m)
E	transfer energy per unit mass of fluid (J/kg)
$E_{r,ex}$	relative error (%)
e	maximum thickness (mm)
F_i	external body force (N/m^3)
g	gravity (m/s^2)
K	coefficient of contraction (dimensionless)
k	turbulent kinetic energy
Q	volumetric flow (m^3/s)
M	mach number
$\dot{m}$	mass flow rate (kg/s)
n	rotational speed (s^{-1})
P	pressure (N/m^2)
P_t	total pressure (N/m^2)
P_p	static pressure (N/m^2)
r	radius (m)
r_m	midspan radius (m)
t	time (s)
T	temperature (ºC)
u	circumferential velocity of the fan (m/s)
v	velocity (m/s)
$\vec{V}$	velocity vector fluid [m/s]
w	relative flow velocity (m/s)
z	number of blades

Subscripts

a	axial
atm	atmospheric
d	dynamic
h	hub
i	vector
j	vector
k	vector
m	meridional
p	static
r	radial
t	tip
t∞	theoretical (∞ blades)
u	tangential
1	inlet
2	outlet

Greek symbols

α	angle between absolute flow velocity and circumferential velocity (degree)
β	angle between relative flow velocity and circumferential velocity (degree)
δ_{ij}	delta tensor
ε	turbulent dissipation
ρ	density (kg/m^3)
Δ	increment
τ_{ij}	Reynolds stress component (N/m^2)
μ_t	turbulent viscosity (m^2/s)

φ mass flow coefficient: $\varphi = \frac{\dot{m}}{n.\rho.D^3}$

Ψ pressure coefficient: $\Psi = \frac{\Delta P}{\rho(n.D)^2}$

1. Introduction

A small axial fan is widely adopted in electronic field. Mainly it is used in a personal computer because of their reliable and simple structures. The cooling fans force the air to flow and at the same time it generates aerodynamic noise. The flow is driven by centrifugal force that cause by fan rotation.

The flow field between the stationary casing and the rotor tip of small axial fan is complex because of the annulus wall boundary layer, the rotor wake and the leakage flow. Shape of blades profile also play an important role in the performance of the fans and their efficiency.

Pressure difference across the blade width generates air flowing through the gap at the blade tip. The tip of the blade has the highest circumferential velocity. The air-gap width and its shape significantly affect integral aerodynamic characteristic and acoustic emission of fan. Problem of the air-gap leakage and generation of the induced swirling have been frequently discussed by different authors.

Passive control technique by modifying end-plate according to the concept of the leakage-vortex rotation number improved the efficiency with increase peak performance [1]. By adding tip end-plate which have geometry of 2 mm width inconstant length of chordwise has decrease vorticity variation on the surface blades. It helps to reduce broadband noise in the far field but not in reducing discrete noise in the near field [2].

Zhang et al [3] studied the effect of the irregular airfoils on the aerodynamics performance of small axial flow fan. Two irregular designs were applied to the normal airfoil. One of them have several convex grooves are bound in blade pressure surface and the other one has a wave-shaped edge which is bound to the blade trailing edge of the fans. The result shows the total pressure of the three airfoils are relatively similar. The performance curve of airfoil that have several convex grooves has a smooth feature. It also changes the turbulent structure near the wall and compress the sphere influence of the vortex while the wave-shaped edge airfoil changes the flow direction of vortex shedding.

Zhang et al [4] present that tip flange of the fan has a certain influence on the characteristics of fan. It contributes to forming tip vortex shedding. The investigation used the numerical simulation and experimental methods to investigate the effect of tip flange on tip leakage flow.

The influence of saw tooth trailing edge serration has been investigated using stereoscopic particle image velocimetry (PIV). It shows that flow will undergoes important changes in various mean flow and turbulence statistic measures [5].

Zhu et al [6] studied aerodynamic performance of small axial flow fan with splitter blade. Static characteristics of small axial fan flow can be improved with splitter blades. Generally, the static pressure rise of axial flow fan with splitter blade is higher than an axial flow fan without splitter blade but the efficiency is closely similar between them.

In this paper, 2 modifications were applied to the airfoils of the fans. Numerical simulation and experiments were performed to analyse the static characteristic and internal flow feature of the small axial fan.

2. Objective

The objective of this work is to find a suitable modification that can be made on the impeller of a small axial flow fan that will affect its aerodynamics problems such as flow speed, viscosity and compressibility. An extensive exploratory literature review was performed in other chapters to explain more details about aerodynamics problems at a theory level. It is very important to know and understand the theory so that it can be applied in our daily life and solve many engineering problems. This project only investigates about a small axial fan. There were already many people have done experiments about a small axial fan but there are many improvements can be made so that our knowledge about this small device can expand. Some simulations and experiments on how air flow through a cooling fan have been made and compared so that the analysis will be more accurate and reliable. The simulation made by using NX10 Siemens PLM Software and experiment was done using a small axial fan.

3. Literature view

3.1 Fan Classification

A fan is an electrical device with an impeller that turns quickly, used to move the air around. Fan also can be defined as a machine or simple turbomachine with rotating blades that move a current of air or gas for cooling or ventilation. Fan produce flows with high volume and low pressure while compressor produces high pressure but low volume. There are several types of fan in the world that can be categorized into axial, radial or centrifugal and mixed-flow fan.

The earliest electric fan appeared late 18th century. They were bipolar and their blades were adapted from the windmill. Usually, there were six pie shaped flat leaves of brass. The speed was controlled by using resistance wire. Sometimes they used light bulbs to act as a resistance wire. Early 19th century, blade design began to change and few modifications started to be applied.

Axial fan is a hydraulic machine that increases the pressure of air or gas that flow through it. Axial fan will suck the air and force the air out parallel to the shaft. Axial fan operates at high specific speed. The design of the fan's blade is one of the main properties that have effect on the pressure created and the suction force that retains the flow across the fan. Power, flow rate, pressure rise and efficiency are normally the main parameters to understand the fan's behaviour.

Axial fans are frequently used in exhaust applications where airborne particulate size is small. It is also useful to generate reverse air flow and it can operate in the opposite direction if needed. Axial fans have a number of advantages over other types of fan which are compact, lightweight, low cost, direct-drive units operating near the synchronous speed of the induction motor and belt-drive units offering flexibility in fan speed selection. Mainly it is used for exhausting contaminated air or supplying fresh air, unidirectional or reversible airflow applications and in exhaust applications where airborne particulate size is small, such as dust stream, smoke and steam.

However, axial fans also have several disadvantages. Axial fans have a stall region in the lower airflow range that makes them unsuitable for system operating widely varying air flow conditions. The airflow capacity for axial fans is lower than centrifugal fans, thus it needs to rotate faster for more airflow capacity and this will cause axial fan to be noisier.

There are several types of axial fans. One of them is the propeller fan or panel fan and this is simplest version. The blades of a propeller act as rotating wings and produce force through the application of Newton's third law, generating a difference in pressure between the forward and rear surfaces of the airfoil-shaped blades. Propeller fan generates high airflow rate at lower pressure, have lower efficiencies, it is a little bit noisy but inexpensive. It can be found everywhere such as in industrial, commercial, industrial and residential applications. It has a lower number of components thus, resulting in lower cost.

The other one is tubeaxial fan, which is a propeller fan placed inside a cylinder. It is connected directly to a motor or driven by a belt. By improving the airflow characteristics, tubeaxial fans achieve higher pressure and better operating efficiencies than a propeller fan. Usually, this type of axial fan is used in medium-pressure, high-airflow rate applications and are well suited for ducted HVAC installations. Tubeaxial fan has moderate airflow noise. Normally, it's used in exhaust applications because it creates sufficient pressure to overcome duct losses and is relatively space efficient. It can accelerate quickly to a certain speed because it has low rotating mass.

Vaneaxial fan is a tubeaxial fan, but with outlet vanes that improve the airflow pattern, converting the airstream's kinetic energy to pressure. The airflow created is comparatively uniform. They have low rotating mass which helps to accelerate quickly to a certain speed. It is used in a medium to high-pressure application such as heat, smoke and fume removal, process drying, comfort and process cooling and general ventilation.

Vaneaxial fan also can generate flow in the reverse direction that is one of its advantages so this type of fan is very useful in ventilation applications. Varying hub-to-tip ratio of a fan will change the fan's performance capabilities. Rotors with higher hub-to-tip ratio will generate higher static pressures while lower hub-to-tip ratios will generate less static pressure. Its blades can be adjusted so angle of attack can be changed. Variable pitch blades can change the load on the fan, thus providing an effective and efficient method of airflow control. The straight-through airflow, minimal discharge vortex and static regain available from a vane axial fan make it a very desirable air moving device. Vaneaxial fans are frequently connected directly to a motor shaft.

3.2 Velocity diagrams

To predict the performance of an axial fan, a deep knowledge of the flow characteristics of the axial fan is needed. To simplify analysis of 3D flow, one-dimensional analysis which focus on the inlet and outlet of the axial is required. Under ideal (design) operating conditions, the velocity diagrams at the inlet and outlet for a fan are illustrated in Figure 3.1. to have maximum energy transfer without whirl at the inlet or outlet.

At the inlet, the air moving with an absolute velocity c_1, enters the axial fan and make an angle $\alpha_1=90^o$. As the air flow is uniform, meridional velocity ($c_{1m} = c_{2m} = c_m$). In the axial flow, radial flow is non-existent. Therefore, the value of tangential velocity (u) that enter and exit the axial fan for the same radius are the same. $u_1 = u_2 = u$.

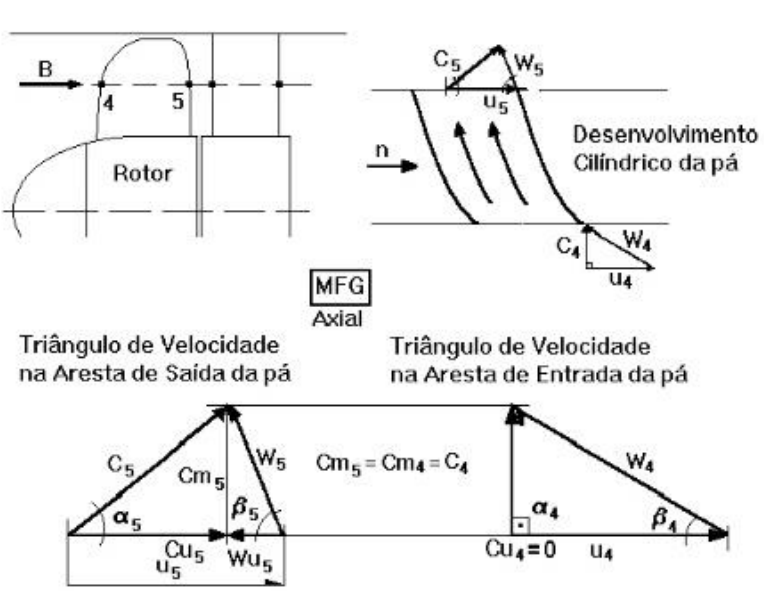

Figure 3.1. Velocity diagrams at the inlet and outlet [7].

The tangential velocity at a point on the axial fan blade due to axial fan rotation is $u=r\omega$. With respect to the impeller, the relative flow velocity can be defined with the vector equation $w = c – u$, where c is the absolute flow velocity and w is a relative flow velocity. The components c and w in the direction of u are tangential-flow velocities which are u_u and w_u. Those normal to u, are called meridional components, c_m and w_m.

The volumetric flow rate through the impeller can be expressed as $Q = c_m.A$, where A is the flow passage area normal to the meridional direction, r_t is radius at the tip and r_h is a radius at the hub.

$$A_1 = A_2 = \pi(r_t^2 - r_h^2)$$

3.3 Euler equation for axial-flow fans

For the study of the Euler equation of axial fans, I have based on the information provided by Peng [8].

For axial-flow machines there is no change in the radial distance from the inlet to the outlet. Considering a mean radius defined as:

$$r_m = \sqrt{\frac{r_t^2 + r_h^2}{2}}$$

Where:
r_m: midspan radius [m]
r_t: tip radius [m]
r_h: hub radius [m]

In one-dimensional flow analysis, the average flow conditions can be treated at this mean radius.

Ideally, the relative flow velocity (w) is tangent to the blade mean line at the inlet and the outlet, that is, $\beta_f = \beta_b$, where the subscripts, f and b, are fluid and blade respectively.

The ideal Euler equation for energy transfer expressed in terms of energy transfer per unit mass of fluid, for a fan is:

$$\Delta E_{t\infty} = c_{2u}.u_2 - c_{1u}.u_1 \qquad [J/kg]$$

or in terms of energy transfer per unit pressure is expressed as

$$\Delta P_{t,\infty} = \rho(c_{2u}.u_2 - c_{1u}.u_1) \qquad [N/m^2]$$

Where:

$\Delta P_{t\infty}$: Pressure [N/m^2]
ρ: density [kg/m^3]
c_U: tangential component of absolute velocity of air [m/s]
u: circumferential speed of the fan [m/s]

Here, $r_1 \approx r_2$, $u_1 \approx u_2$, and therefore:

$$\Delta P_{t,\infty} = \rho u(c_{2u} - c_{1u}) = \rho u \Delta c_u \qquad [N/m^2]$$

3.4 Three-dimensional flow effects: radial equilibrium requirement

The flow through a rotating impeller in general is a complicated three-dimensional process. The three-dimensional flow generates effect such as secondary flow, boundary layer on the hub and casing surfaces and leakage through the tip clearance which affect the total pressure loss.

The tangential-flow velocity distribution is another important three-dimensional flow effect. This can be controlled in the axial fan design by selecting a proper blade section setting along the radius.

The general three-dimensional momentum equation of inviscid fluid in a radial direction expressed in a cylindrical coordinate system is:

$$-\frac{1}{\rho}\frac{\delta p}{\delta r} = C_r\frac{\delta C_r}{\delta r} + \frac{C_u}{r}\frac{\delta C_r}{\delta \theta} + C_a\frac{\delta C_r}{\delta z} - \frac{C_u^2}{r} \qquad (\mathrm{kg/m^2s^2})$$

Where:
c_r: radial component of the absolute velocity (m/s)
c_u: tangential component of the absolute velocity (m/s)
c_a: axial component of the absolute velocity (m/s)
r: radius(m)
$\delta p/\delta r$: gradient of the radial pressure ($\mathrm{kg/m^2s^2}$)

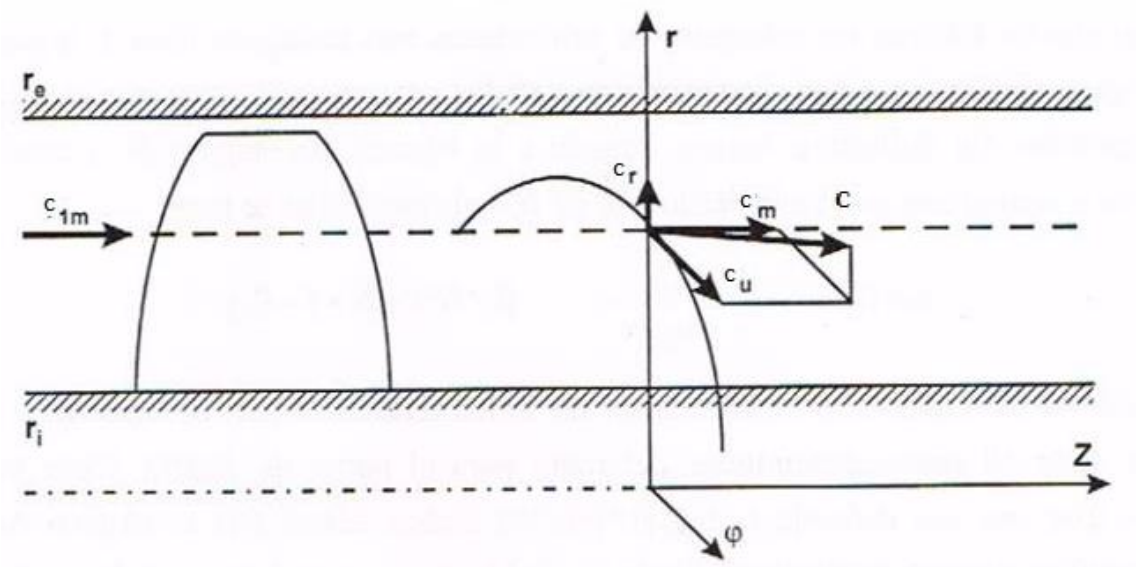

Figure 3.2. Radial equilibrium requirement [9].

If it is assumed that the radial component is zero or negligible, catching the movement of particles in a fluid is made coaxial cylinder as shown in the Figure 3.2. For that to happen, the pressure gradient in the direction radius must counteracting the centrifugal force of the particle.

$$\frac{1}{\rho}\frac{dp}{dr} = \frac{C_u^2}{r}$$

The equation above is called the radial equilibrium condition that can also be derived from the force balance between the pressure gradient and the centrifugal force of a fluid element in the radial direction.

The momentum equation can also be written along a streamline (neglecting the radial-flow velocity component) as:

$$\frac{dp}{\rho} + C_u . dC_u + C_a . dC_a = 0$$

Combining the last two equations:

$$\left(\frac{C_u}{r}\right) d(C_u r) + C_a . dC_a = 0$$

Several different tangential-flow velocity distributions along the radius can satisfy this momentum equation:

- **Free-vortex flow** (C_u.r = constant.). It is the simplest type of velocity distribution. The flow coming out of the machine axial must have a distribution of velocity, c_u, which meets C_u.r = constant. (i.e a kinetic moment uniform), so the tangential velocity varies inversely with the radius, forming what is called the free vortex. It also results in uniform loading along the impeller radius from hub to tip, since

  $$\Delta \mathrm{E} = \mathrm{u}.\mathrm{C_u} = \omega . r . \mathrm{C_u} = const.$$

  The flow meets the free vortex law, $\mathrm{C}_u \mathrm{r}$ = constant, upstream and downstream of the rotor. Each element of the blade performs equal work. The axial velocities over the blades are virtually constant. The blade chord at the tip is usually reduced whilst the twist near the hub can be substantial.

- **Forced-vortex flow** can be generalized as $C_u.r^n$ = const. The value of n is 1 for free-vortex flow, and n = -1 for the called forced-vortex or solid-body rotation because its tangential velocity distribution is the same as that of a rotating solid body. The chord strongly increases with increasing radius. The work performed by the blades is maximized at their tips leading to the large tip chords when compared with the roots of the blades. A truly forced vortex design would require minimum tip gaps between blades and the casing. Weight would also increase towards the periphery leading to a greater centrifugal stress.

- **Arbitrary vortex.** It is intermediate vortex between the previous types of vortex. It also does not require radial equilibrium and a real velocity distribution can be applied for designing process. Blades have to be cut away near to their roots so that they do not interfere with each other. The exact nature of the vortex formation depends of the blade design laws, blade geometry and the operating condition. In general, higher aerodynamic performance can be attained by using arbitrary vortex method.

3.5 Contraction coefficient

The thickness of blades is not zero, therefore the velocity of air flow that pass through the axial fan is greater. If e(r) is the maximum thickness of the blade for the radius r, and Z is the number of blades, c is the theoretical axial velocity and the corrected axial velocity, C_1. To calculated C_1, the equation used was;

$$C_1(corrected) = c\frac{1}{K}$$

$$K = 1 - \frac{z.e(r)}{2.\pi.r}$$

Where K: coefficient of contraction [dimensionless]

3.6 Mass flow coefficient

Flow coefficient is a dimensionless parameter that described relationship of the suction flow rate to impeller diameter and rotational speed.

$$\varphi = \frac{\dot{m}}{n.\rho.D^3}$$

Where $\dot{m}$: mass flow rate [kg/s]
n: rotational speed [s^{-1}]
D: diameter [m]
ρ: air density [kg/m^3]

3.7 Static pressure coefficient

Static pressure coefficient is a dimensionless parameter. It describes relative pressure in the flow field.

$$\Psi = \frac{\Delta P}{\rho(n.D)^2}$$

Where ∆P: different of static pressure [Pa]
ρ: air density [kg/m^3]
n: rotational speed [s^{-1}]
D: diameter [m]

4. Study of fan

4.1 General data

A small axial flow fan, LYF DC 12V 4PIN 8cm 8015s brushless was selected as the sample fan in this paper. The rotor has 7 rotor blades. The main parameters of the prototype are shown in Table 4.1. and Table 4.2. shows its specifications.

Outer casing diameter	78 mm
Blade tip diameter	76 mm
Rotor hub diameter	34.5 mm
Tip clearance	1 mm
Blade span height	20.75 mm
Blade pitch	15.48 mm
Blade chord length	23 mm
Hub-to-tip ratio	0.45
Blade geometry	circular-arc
Blade number	7

Table 4.1. Main parameters of the prototype fan.

Power connector	4 pins
Voltage	12V
Rated current	0.18A
Air flow	45CMF
Air speed	3.4m/s
Fan speed	1900RPM±10%
Bearing style	Sleeve
Noise level	25dbA±10%
Weight	40g
Fan size	80x80x15mm

Table 4.2. Main specifications of the prototype fan.

Figure 4.1. Prototype pictures [10].

4.2 Theoretical study

In this section, the theoretical study about velocities diagrams and distribution of pressure was carried out by using geometries of blades (Table 4.1.) and fan operation data (Table 4.3.), considering the design conditions (Table 4.4.). Fan speed in this section is n = 2000 rpm. This rotational speed was obtained by using tachometer. The β

angle of the blade measured at the inlet and outlet of the fan. Table 4.5. shows β angle for 3 sections which are at hub, midspan and tip of blade.

	HUB	MIDSPAN	TIP
Q (m^3/s)	0.0061	0.0118	0.0152
P_t (Pa)	12.92	34.64	51.97
P_d (Pa)	5.31	13.04	17.70
P_p (Pa)	7.62	21.63	34.32

Table 4.3. Fan operation data.

	HUB	MIDSPAN	TIP
β_1	25°	28°	28°
u_1 (m/s)	3.61	6.18	7.96
Area (m^2)	0.0036	0.0036	0.0036
$c_m=c_1$ (m/s)	1.68	3.29	4.23
w_1 (m/s)	3.99	7.00	9.01
c_{1u} (m/s)	0	0	0
β_2	69°	65°	59°
u_2 (m/s)	3.61	6.18	7.96
c_{2m} (m/s)	1.68	3.29	4.23
w_2 (m/s)	1.80	3.63	4.94
c_{2u} (m/s)	2.97	4.65	5.42
c_2 (m/s)	3.41	5.69	6.87

Table 4.4. Inlet and outlet velocities (design conditions).

	HUB	MIDSPAN	TIP
Angle β_1	25º	28º	28º
Angle β_2	69º	65º	59º

Table 4.5. Angle of various sections of blade.

4.2.1 Velocity diagrams

In order to obtain the maximum energy transfer, the tangential-flow velocity to the inlet section to the impeller must be zero (α_1 = 90º). Therefore, $c_1=c_{1m}$.

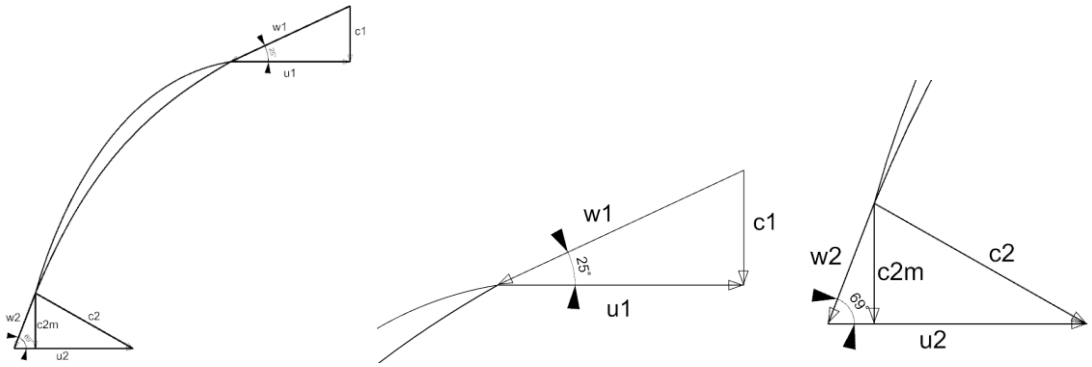

Figure 4.2. Velocity diagram of inlet and outlet at hub.

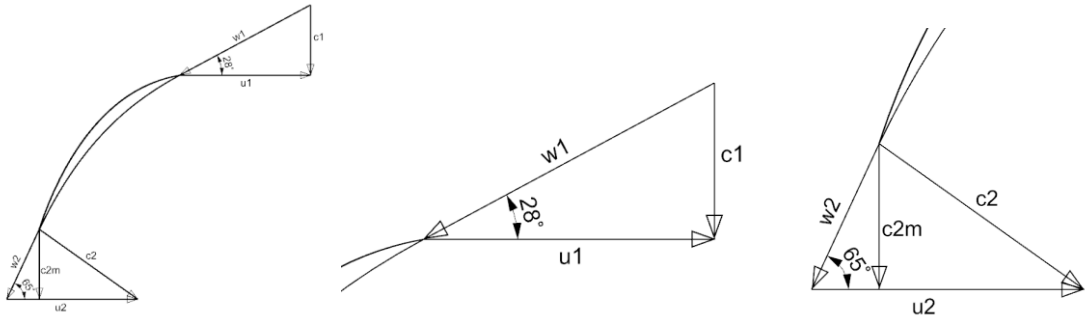

Figure 4.3. Velocity diagram of inlet and outlet at midspan.

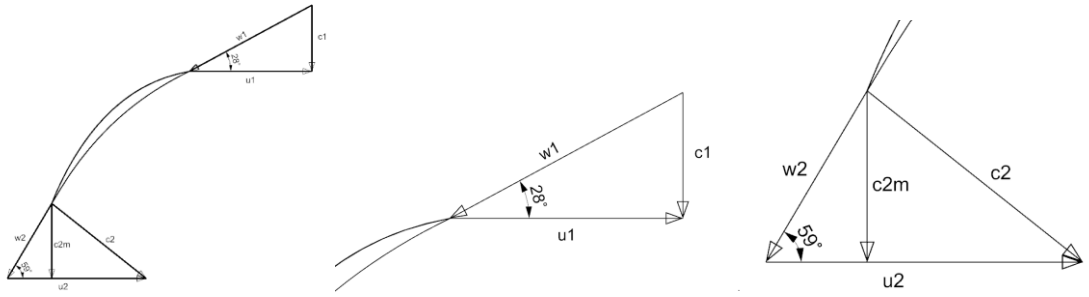

Figure 4.4. Velocity diagram of inlet and outlet at tip.

With the data of velocities shown by velocities diagrams, and to know more about the behaviour of the axial fan, the design condition can be determined as close as possible, regarding the radial equilibrium condition (section 3.4).

Considering the equilibrium equation $C_u.r^n$ = const, the logarithm is:

$$\mathrm{LN}\,(\mathrm{Cu}) + \mathrm{nLN(r)} = \mathrm{LN(const)}$$

The Figure 4.5. shows the logarithm of the tangential component of absolute velocity with respect to logarithm of radius. Creating linear line with coefficient R^2=0.9948, gives the expression:

$$\mathrm{LN}\,(\mathrm{Cu}) = 4.238 + 0.774 * \mathrm{LN(r)}$$

The condition of equilibrium equation shown by the axial fan for the rotational speed of 2000 rpm is:

$$C_u r^{-0,774} = 69.269$$

Where n = - 0,774

	ln r	ln C_{2u}(m/s)
HUB	-4.06	1.09
MIDSPAN	-3.52	1.54
TIP	-3.27	1.69

Table 4.6. values of ln r and ln C_{2U}

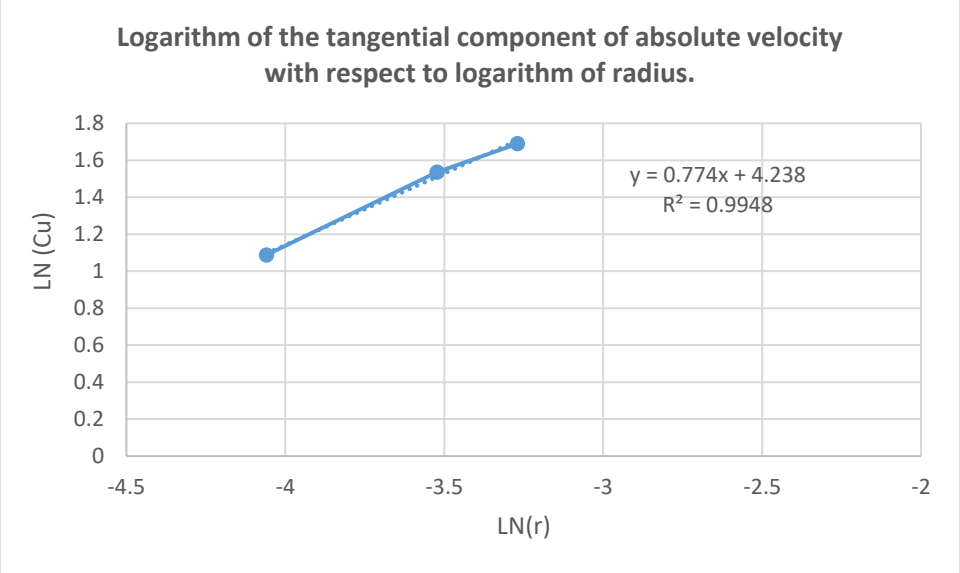

Figure 4.5. Logarithm of the tangential component of absolute velocity with respect to logarithm of radius.

4.2.2 Pressure distribution

Theoretical pressure distribution along the blade, from hub to tip was obtained from the diagram of velocities and some calculations were made. The table 4.7. shows the total pressure, dynamic pressure and static pressure.

To calculate the total pressure, Euler's equation was used:

$$P_t = \left(\frac{u_2.c_{2u} - u_1.c_{1u}}{g}\right) \times g \times \rho_{air} \ [\text{Pa}]$$

or

For dynamic pressure:

$$P_d = \left(\frac{c_2^2 - c_1^2}{2g}\right) \times g \times \rho_{air} \ [\text{Pa}]$$

And for static pressure:

$$P_p = \left(\frac{u_2^2 - u_1^2}{2g} + \frac{w_1^2 - w_2^2}{2g}\right) \times g \times \rho_{air} \ [\text{Pa}]$$

Where:

g = 9.8 m/s^2

ρ_{air} = 1.207 kg/m^3

	HUB	MIDSPAN	TIP
Total Pressure (Pa)	12,92	34,67	51,97
Dynamic pressure (Pa)	5,31	13,04	17,70
Static pressure (Pa)	7,62	21,63	34,32

Table 4.7. Values of theoretical pressures.

The Figure 4.6. shows the lineal distribution of the pressure along the blade from hub to tip.

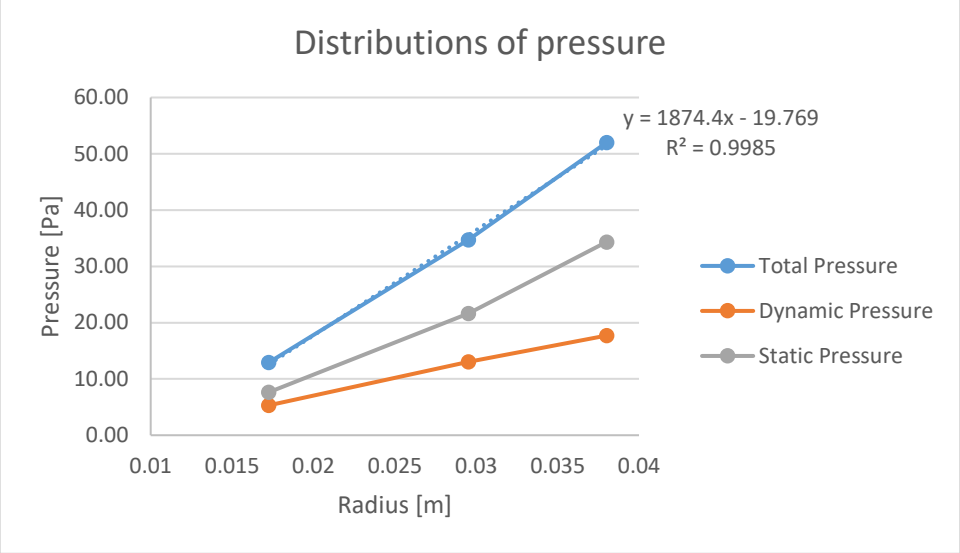

Figure 4.6. Distribution of pressure.

4.2.3 Contraction coefficient

The thickness of blades is not zero, therefore the velocity of air flow that pass through the axial fan is greater. If e(r) is the maximum thickness of the Blade for the radius r, and Z is the number of blades, the axial velocity is:

$$C(corrected) = c\frac{1}{K}$$

$$K = 1 - \frac{z.e(r)}{2.\pi.r}$$

Where K is a coefficient of contraction.

	e(r) [mm]	Radius [mm]	z	K	c [m/s]	C [m/s]
HUB	0.96	17.25	7	0.938	1.68	1.79
MIDSPAN	1.08	29.5	7	0.959	3.29	3.43
TIP	1.16	38	7	0.966	4.23	4.38

Table 4.8. Values of coefficient of contraction.

4.2.4 Mass flow coefficient

By using equation at section 3.5, mass flow coefficient was calculated and the data were put together on the Table 4.9.

$\dot{m}$ (kg/s)	Flow Coefficient (φ)
0.0130	0.086
0.0185	0.123
0.0193	0.129
0.0242	0.161
0.0255	0.170

Table 4.9. Values of flow coefficients.

4.2.5 Static pressure coefficient

Static pressure coefficient for various values of static pressure were calculated using equation at section 3.6 and the results were put together on the Table 4.10.

ΔP_s [Pa]	Pressure coefficient (Ψ)
6.848	0.046
6.848	0.046
5.869	0.039
5.869	0.039
4.891	0.033

Table 4.10. Values of pressure coefficients.

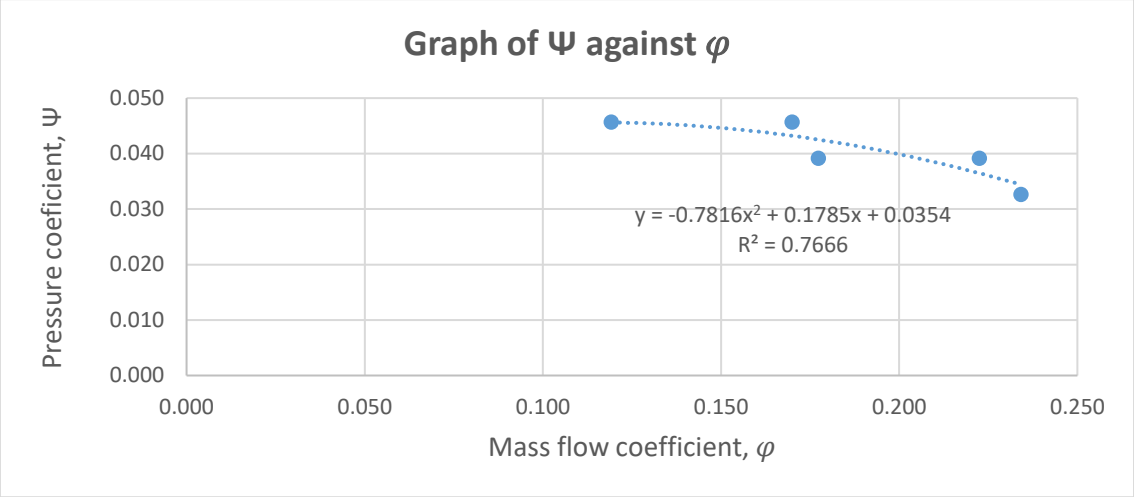

Figure 4.7. Graph of Ψ against φ.

4.3 Experimental measurements

4.3.1 Rotational velocity

To measure axial fan rotational speed, a Lutron digital tachometer (DT-2236) was used. The measurements were repeated on several occasion and axial fan was maintain to rotate for 1 minute before the measurement was taken. The axial fan speed was n = 2000 rpm. Figure 4.8. shows the axial fan and how the measurement was taken.

Figure 4.8. Pictures of how fan rotational speed was measured.

4.3.2 Static pressure

The voltage was set at 12 V and the current was 0.18 A by using Power Supply FAC-662B PROMAX. A hole was made on the polystyrene and an axial fan was put into it as shown in the Figure 4.9. After that, it was connected between two pipes and sealed completely to prevent air leakage (Figure 4.10), so that the reading of manometer will be more accurate. An anemometer PCWI (model GVA 0430) was used to measure average velocity of air flow that pass through the pipe.

The values of air flow (Q) were calculated by using:

$$Q = \frac{\pi D^2 V}{4} \quad [m^3/s]$$

Where; Diameter of pipe (D) =0.0846m

∆P (mmH2O) is a different of static pressure at inlet and outlet. The values of ∆P for different airflow were taken at inclined manometer. After all the values were taken and recorded on the Table 4.8, the line graph (Figure 4.10.) was plotted to see how the different of static pressure was affected by airflow.

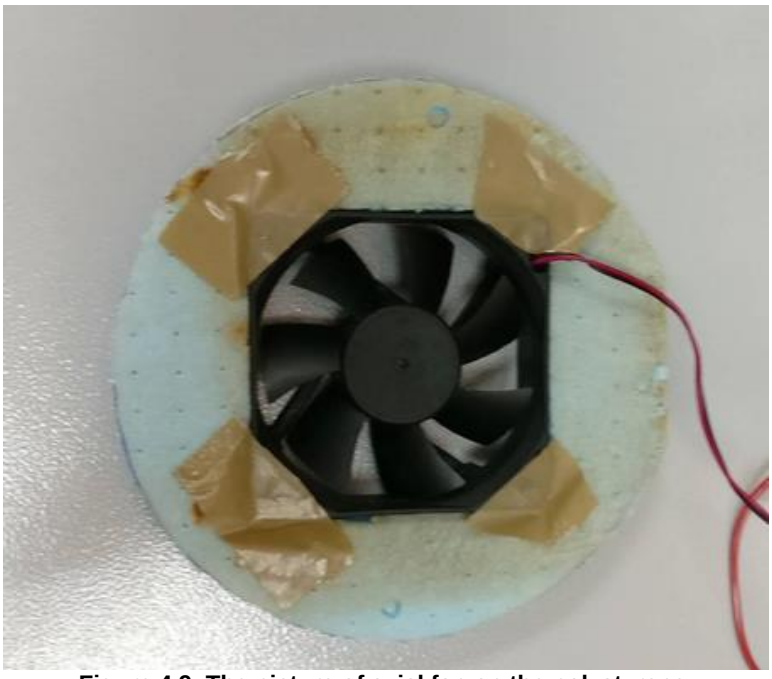

Figure 4.9. The picture of axial fan on the polystyrene.

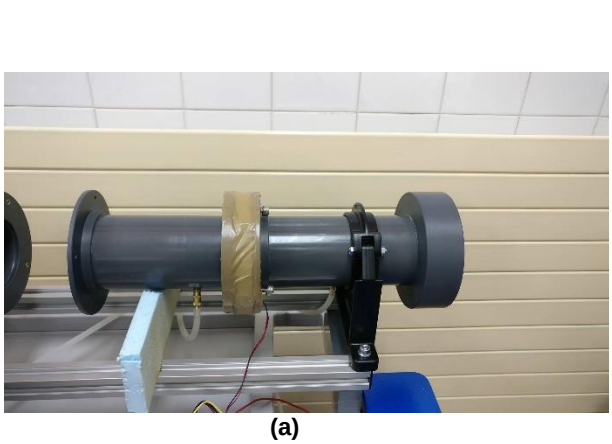

(a)

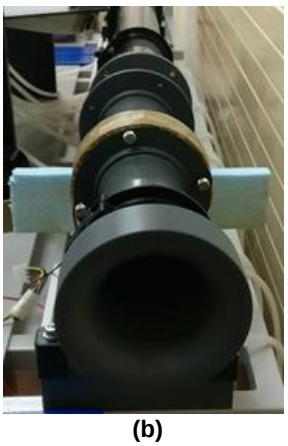

(b)

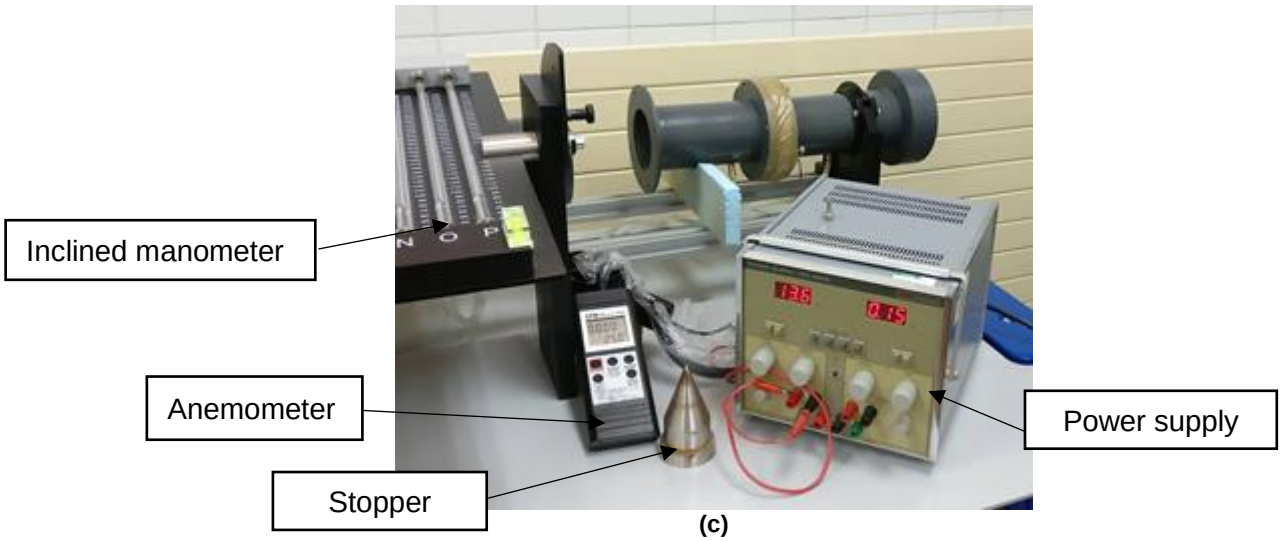

(c)

Figure 4.10. (a), (b) and (c) shows the pictures how the experiment was set up.

V (m/s)	Q (m^3/s)	$\dot{m}$ (kg/s)	φ	ΔP (mmH2O)	ΔP_s [Pa]	ψ
1.95	0.0110	0.0130	0.086	0.7	6.848	0.046
2.78	0.0156	0.0185	0.123	0.7	6.848	0.046
2.90	0.0163	0.0193	0.129	0.6	5.869	0.039
3.64	0.0205	0.0242	0.161	0.6	5.869	0.039
3.83	0.0215	0.0255	0.170	0.5	4.891	0.033

Table 4.11. Values of velocities, airflows and different of static pressure.

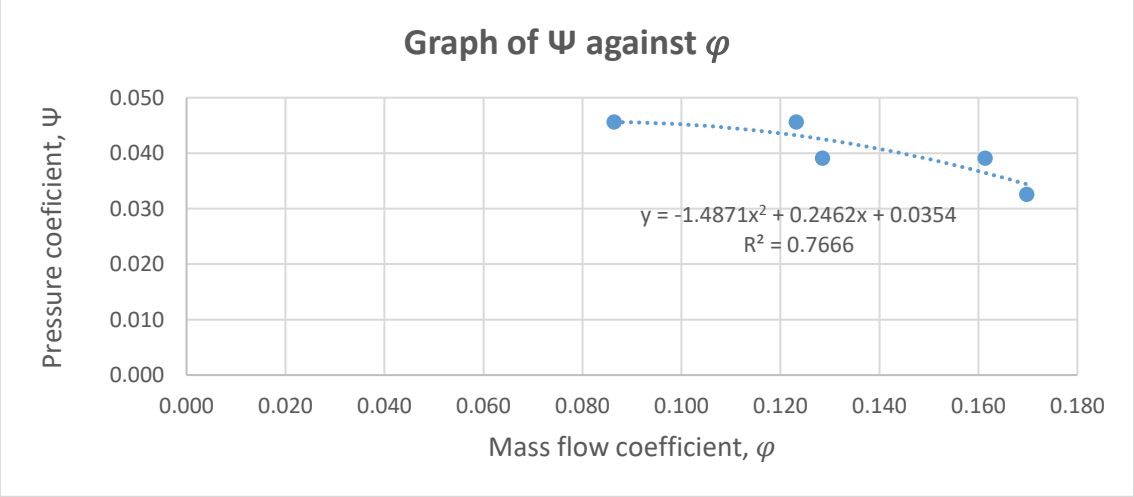

Figure 4.11. Graph of Ψ against *φ*.

The results that were obtained during the experimentation for measuring the different of static pressure for the different flow were not very reliable because the measurement apparatus have low precision, therefore it can't be used to validate the model even though the experiment have been carried out.

4.3.3 Velocity

Inlet speed and outlet speed at various points based on Figure 4.12 were measured using an anemometer. As we can see at Table 4.12. and Table 4.13. the speeds of airflow were different at different points.

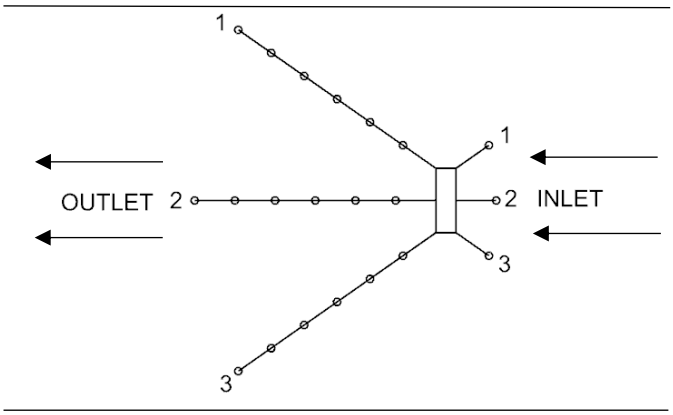

Figure 4.12. Points where the anemometer was placed during the measurement.

Distance (cm)	1	2	3
5	0.66 m/s	1.18 m/s	0.66 m/s

Table 4.12. Inlet velocities at the different points

Distance (cm)	1	2	3
5	1.7 m/s	2.8 m/s	1.15 m/s
10	1.3 m/s	2.6 m/s	1.03 m/s
15	0.85 m/s	1.95 m/s	0.95 m/s
20	0.75 m/s	1.4 m/s	0.93 m/s
25	0.63 m/s	1.15 m/s	0.83 m/s
30	0.5 m/s	0.96 m/s	0.75 m/s

Table 4.13. Outlet velocities at different points.

5. Study of modifications

Optimizing fan blade structure or airfoil is considered to be an ideal modification that can reduce airflow turbulence, increase the performance of blade and improve the aerodynamic performance of small axial flow fan. Many studies on the effect of modification on the blade structure and surface had been done by various authors. Here are 2 types of modifications which were studied and investigated in this project.

5.1 Modification 1

The static pressure difference between the suction and the pressure side of the impeller blades produces a secondary flow over the tip of the rotor-blade. The effect of the addition of winglet to the end of blade was studied. The winglet will be located in the suction surface of the blade (Figure 5.1).

Figure 5.1. A Cooling fan with a winglet [11].

Many investigations on effect of tip end-plate (winglet) on small axial fan were done using experiment method and numerical solution. Passive control technique by modifying end-plate according to the concept of the leakage-vortex rotation number improved the efficiency with an increase peak performance [1]. By adding tip end-plate (winglet) which have geometry of 2 mm width inconstant length of chordwise has decrease the vorticity variation on the surface blades. It helps to reduce broadband noise in the far field but not in reducing discrete noise in the near field [2].

Based on [1] and [2], the modification by adding tip end-plate can be done and investigate in this project. Figure 7.2. shows the blades of modified models in article [2]. But the geometry of the tip end-plate in this project is slightly different. The geometry of the modification that can be made is 2 mm width which is in-constant along the chordwise.

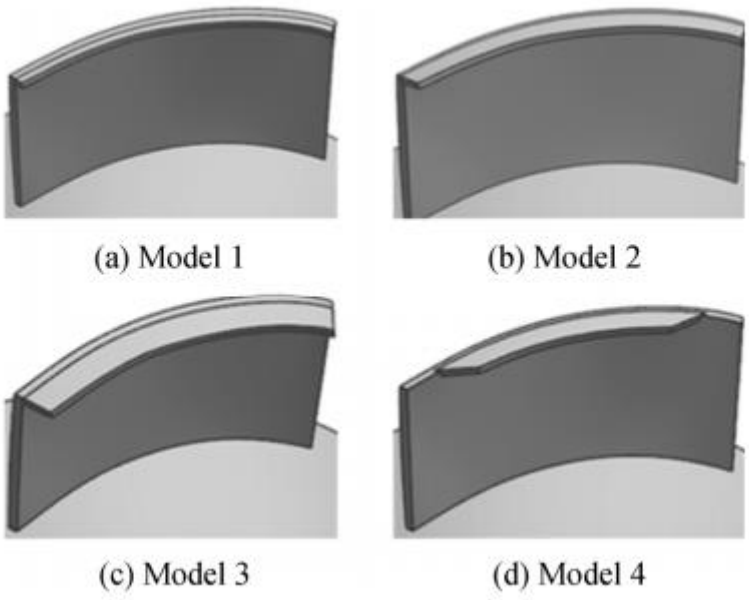

Figure 5.2. Blade of modified models [2].

5.2 Modification 2

It is said in [12] shark fin blade can reduce the effect of turbulence on the blade surface during fan rotation. Therefore, the airflow increases and reduce the vibration on the blade surface. In the Figure 5.3, it can be seen there are 3 shark fins on the blade surface and a winglet at the tip of blade. But in our case, we modify it a little bit different because there are some restrictions that cannot be overcome.

Figure 5.3. Shark fin blade case fan [12].

6. Modeling and Simulation processes

6.1. Modelling process

NX10 Siemens PLM Software was used to design a cooling fan from a prototype. NX10 Siemens PLM Software is a fully associative CAD/CAM/CAE applications. It touches the full range of development processes in product design, manufacturing and simulation. The prototype of the cooling fan was bought from the electronics shop.

All the measurement needed such as diameter, blade thickness, number of blades, chord, stagger angle and etcetera were measured before the designing and modelling process. It took a long time to be able to get the correct measurements because the cooling fan is so small and the same measurement needed to be repeated for several times to avoid human error so that the design model will be same as the prototype. All of these were need to be taken seriously because a little error can cause a different result between simulation and experimentation. All the measurements were taken using millimetre (mm).

The modelling process was done by using NX10 Siemens PLM Software and consisted several processes from 2D drawing to 3D modelling into meshing and simulation. The process of modelling the fan assembly can be divided into 4 processes which are:

- modelling of the three-dimensional solid hub
- modelling of the two-dimensional and three-dimensional blade profile
- modelling of the three-dimensional frame of a cooling fan
- assembling of the complete model of a cooling fan

6.1.1 Modelling of the three-dimensional solid hub

This is the first part in the design of the model and one of the easiest. First, the 2D design of the prototype was done by using the sketch. The diameter of the hub was 34.5mm. Then, it was extruded for 16mm.

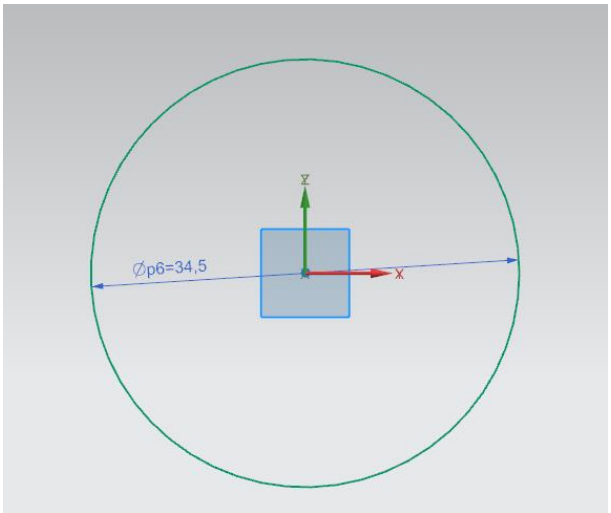

Figure 6.1. Modelling of the three-dimensional solid hub. The diameter of the hub is 34.5mm.

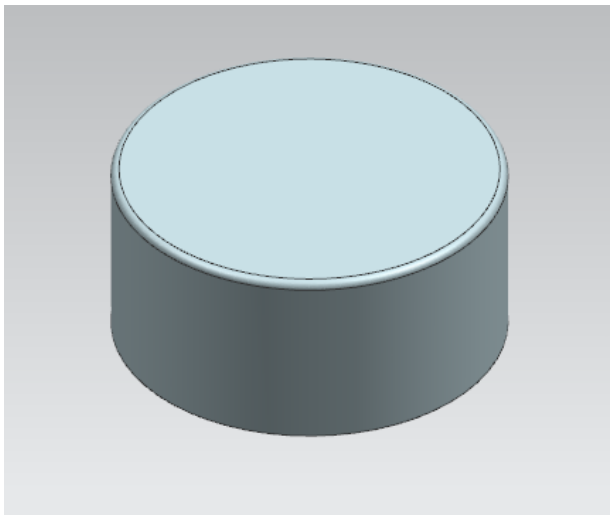

Figure 6.2. Three-dimensional solid hub.

6.1.2 Modelling of the two-dimensional and three-dimensional blade profile

To sketch two-dimensional blade is the most important and the hardest task. The measurements that have been taken to design blade profile were the angle, blade chord length, blade span height and blade pitch. The blade profile has a critical effect on the result. This rotor has 7 blades, its tip diameter is 76mm and its hub-to tip ratio is 0.45. The tip clearance is 1mm. Its specifications are shown in Table 4.1.

The curve on the surface was used to create a surface spline feature directly on a hub surface. Studio spline also was used because it is dynamically created and edits splines by dragging defining points or poles, and assigning slope or curvature constrains at definite points. It was very helpful to create an arc for the blade profile.

Studio surface was used to create the blade profile surface and after that, a solid blade profile can be made. The rotor has 7 blades, rotor so pattern feature was used because it can copy feature into many patterns or layouts with various options for pattern boundary, instance orientation, clocking and variance. Circular layout was used to create other blades. Finally, 7 blades have formed, now all of them can be unite with the hub.

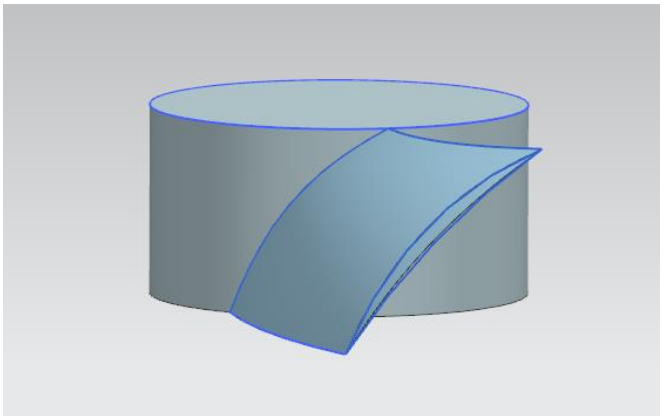

Figure 6.3. Side view of the impeller with 1 blade.

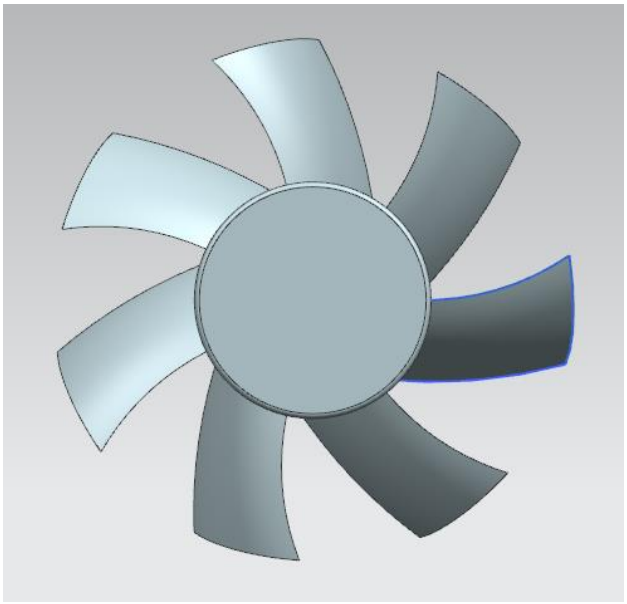

Figure 6.4. Top view of the 3D impeller.

6.1.3 Modelling of the three-dimensional frame of a cooling fan

The frame of a cooling fan also very important because air will flow through it during the simulation process. Any errors during the measurement and designing process will cause an error in simulation process and we need to reduce the error as little as possible. Frame size is 80x80x25mm. First, 2D design was made from a sketch before making it to 3D design.

For the 2D design, a square was sketched. It has length and width 80mm, then was extruded for 25mm thick. Then, circle on the surface was sketched and extruded for 25 mm thick to make a hole. After that, chamfers were made at the edge of the hole. Once finish at the front part, edges were blended, at the back side. Then, bone of the frame was sketched on the back and extruded it 2.5mm thick. A stator that holds the hub at the centre of the bone was sketched and extruded to form 3D. After that, all the components were united to form a frame.

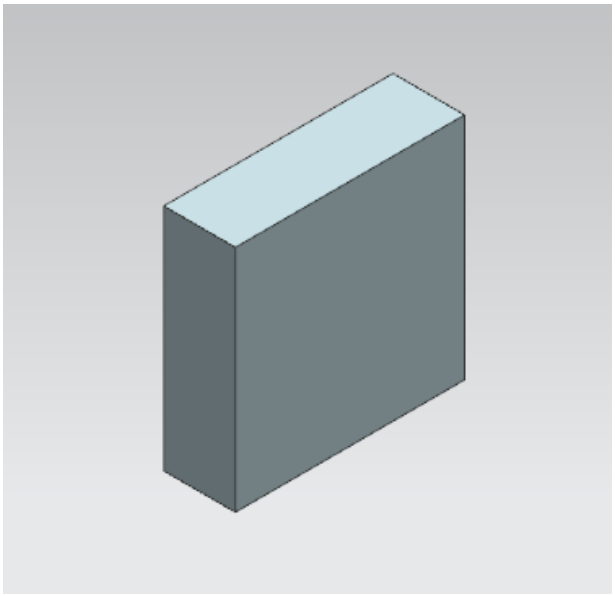

Figure 6.5. Isometric view of the frame before hole is made.

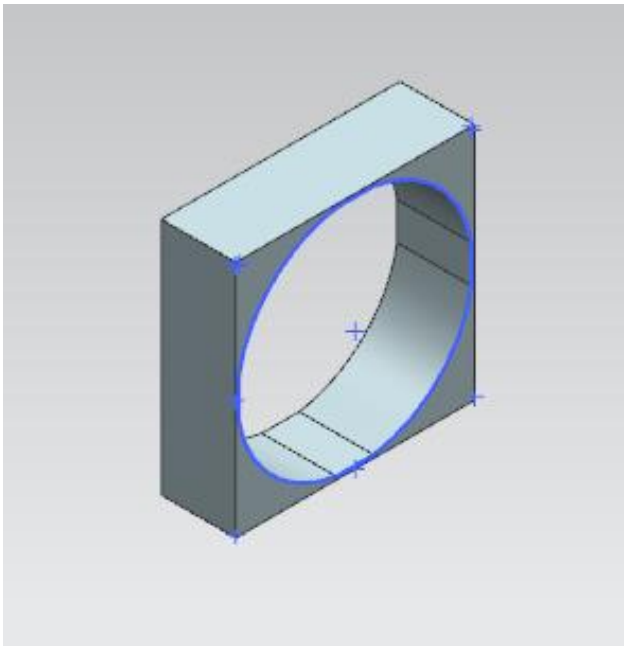

Figure 6.6. Isometric view of the frame after the hole was made.

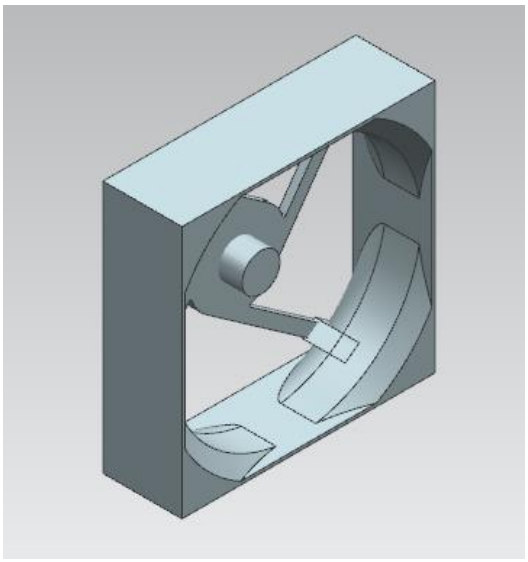

Figure 6.7. Isometric view of finished frame modelling.

8.1.4 Assembling of the complete model of a cooling fan

After finishing modelling the blade and the frame, both of the components can be assembled in the assemble file in NX10 Siemens PLM Software. The assemble process is the final part of the modelling before simulation process. Both components were added in the assemble file and after that, use the assembly constraint that will connect them. There are many different ways to assemble the component together and concentric type of assembly constraint was used because there were only two components and it is the easiest way to assemble them together.

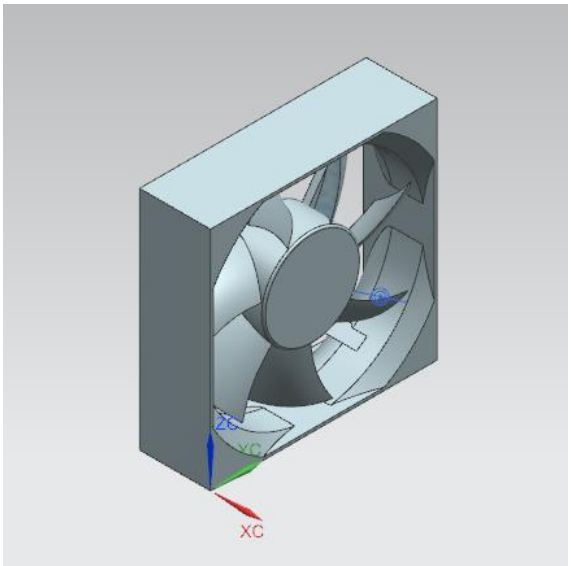

Figure 6.8. Complete assembly of a cooling fan.

6.2 Simulation

6.2.1 Governing equations

The continuity equation and the Navier-Stokes equations are needed to obtain the pressure and velocity around the flow field. For incompressible flow are as follows:

6.2.1.1 Continuity equation

In Cartesian coordinates, continuity equation is:

$$\nabla \cdot \vec{V} = 0$$

Where:

$\vec{V}$: velocity vector of the air flow [m/s]

6.2.1.2 Navier-Stokes equation

Conservation of momentum (Navier-Stokes Equations) for incompressible flow is:

$$\rho g_i + F_i - \nabla p + \nabla \cdot \tau_{ij} = \rho \frac{D\vec{v}}{Dt} \qquad [N/m^3]$$

Where:

ρ: density fluid [kg/m^3],

$\vec{V}$: velocity vector fluid [m/s]

p: pressure [N/m^2]

g_i: gravity [m/s^2]

τ_{ij}: Reynolds stress component [N/m^2]

F_i: external body force [N/m^3].

6.2.2 Computational domain

The computational domain for the simulation consists of the rotating fluid area, the inlet and outlet ducts. For the simulation purposes, the length of the inlet duct is 40mm and the diameter is 200mm while for the outlet duct is 400mm length and the diameter is 200mm as shown in Figure 6.9. The fan hub was set as the coordinate origin.

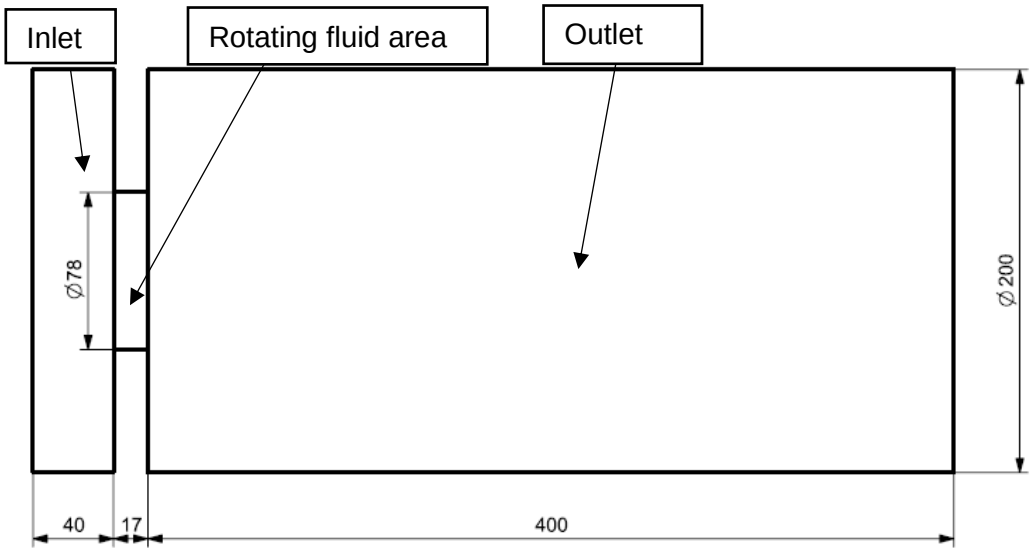

Figure 6.9 Computational domain.

6.2.3 Mesh

Simulation process was done by using NX10 Siemens PLM Software. Advance Simulation application was used because it provides comprehensive tools for finite element modelling and results visualization. Finite element method (FEM) or finite element analysis (FEA) is a numerical method to solve very complex structure, fluid, and multiphysics problems and it only can find a solution that approximates the exact solution. It is the dominant discretization technique in structural mechanics.

A finite element (FE) model comprises a system of points, called “nodes”, which form shape of design. The response of each element is expressed in term of finite number of degrees of freedom characterized as the value of an unknown function, or functions, at a set of nodal points. The density of the finite element mesh may vary throughout the material, depending on the anticipated change in stress. FE model can be created using one-dimensional (1D beam), two-dimensional (2D shell) or three-dimensional (3D solid) elements. The response of the mathematical model is then considered to be approximated by that of the discrete model obtained by connecting or assembling the collection of all elements.

Meshing can be divided to two types, coarse and fine. Coarse meshing is very fast computation and not concerned about stress concentrations, singularities, or warping. Fine meshing is for the best approximation but it takes long time for computation.

The NX software was used to generate the grid for the computational domain. 4-noded tetrahedral element (TET4) was used to mesh all the element in the rotating fluid area and in the regions of the inlet and outlet ducts as shown in Figure 6.10.

Large size of elements was used in flow simulation, as shown in Figure 6.11. to verify if the solution is element size independent or not. An element counts larger than 41000 does not produce a visible different in average velocity of rotating fluid area.

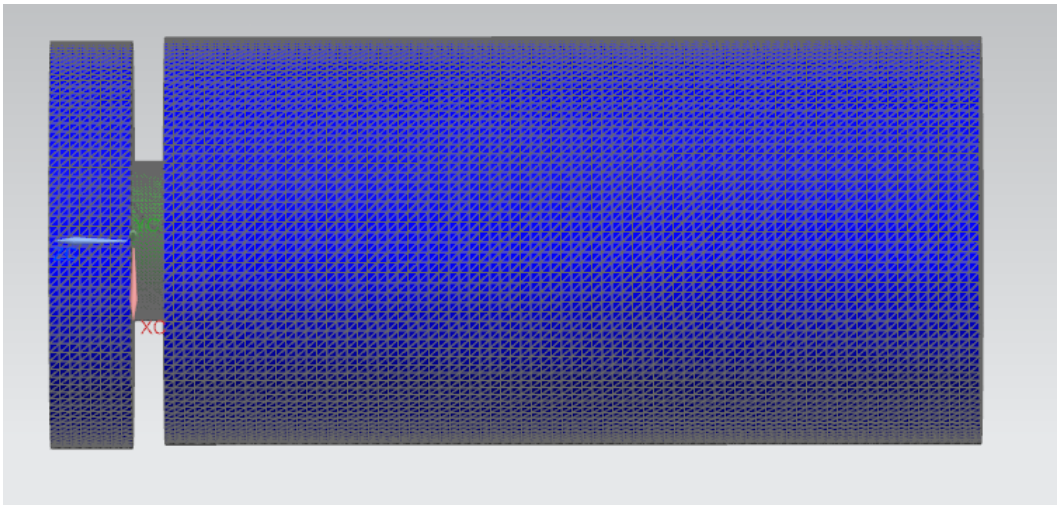

Figure 6.10. Mesh.

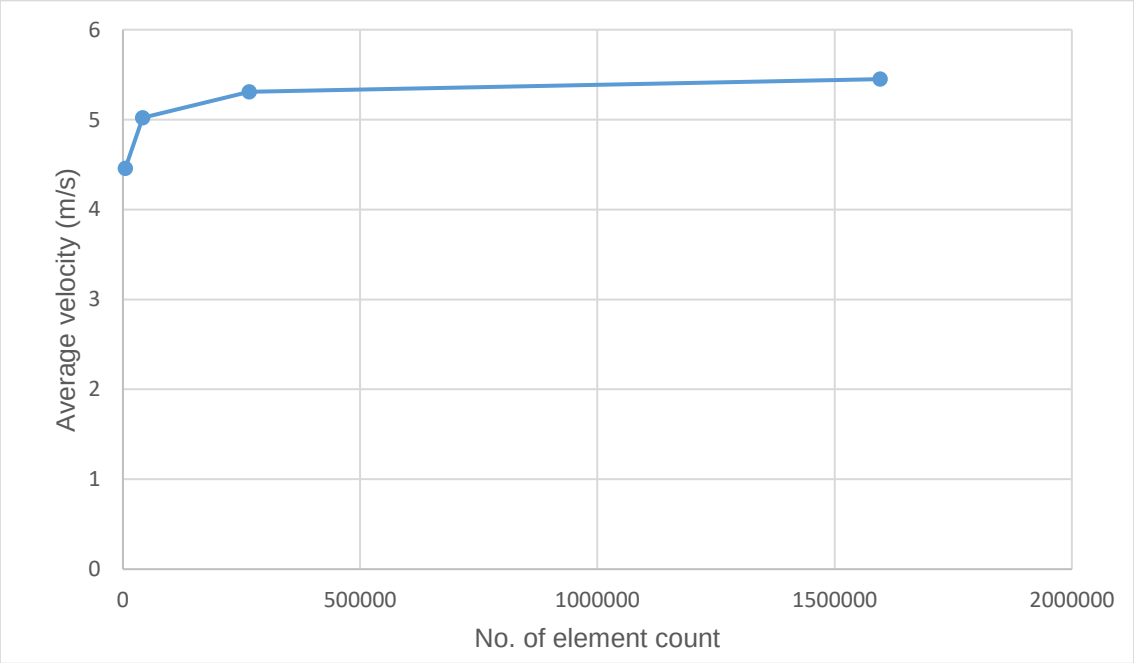

Figure 6.11. Element sensitivity test result.

For the rotating fluid area, element size is 2mm and the material is air. While for the fan, element size is 2mm and the material is ABS. For the inlet and outlet ducts, element size is 5mm and the material used was air. Table 6.1. shows the number of element count of different sections.

Section	Element counts
Inlet duct	42855
Outlet duct	201768
Rotating area	44675
Fan	14107

Table 6.1. Element counts of different sections.

6.2.4 Initial conditions

The ambient conditions in the simulation were considered constant and the values are:

Temperature: T=20ºC

Atmospheric pressure: P_{atm} = 101351N/m^2

Air density: ρ = 1.207 kg/m^3

The air density was considered constant; therefore, it is incompressible fluid. As we see in the literature view section 6.2, the theoretical absolute velocity of fluid at the tip of the blade is 6.78 m/s. With the temperature is 20ºC, the Mach number at the tip of blade is 0.02M, which is inferior to the limit of incompressible fluid (0.3M).

The rotational velocity of rotating body used in the simulation was 2000 rpm which is same with rotational velocity that have been measured experimentally. The rotational velocity was constant for all the time during the simulation process.

6.2.5 Boundary conditions

Every simulation was performed with same boundary conditions. Flow boundary condition for inlet duct is set as an opening and outlet duct have outlet mass flow which is $\dot{m}$=0.0242 kg/s. It external condition is ambient, external pressure type is absolute and external absolute pressure is ambient. Mixing plane simulation object was used to interface fluid regions between inlet duct, rotating fluid area and outlet duct. For the rotating fluid area, moving frame of reference simulation object was used to model the effect of rotating fan on the surrounding fluid. The rotation velocity used was 2000 rpm. The solid wall such as vane surface and hub satisfy the no-slip condition in the computational domain.

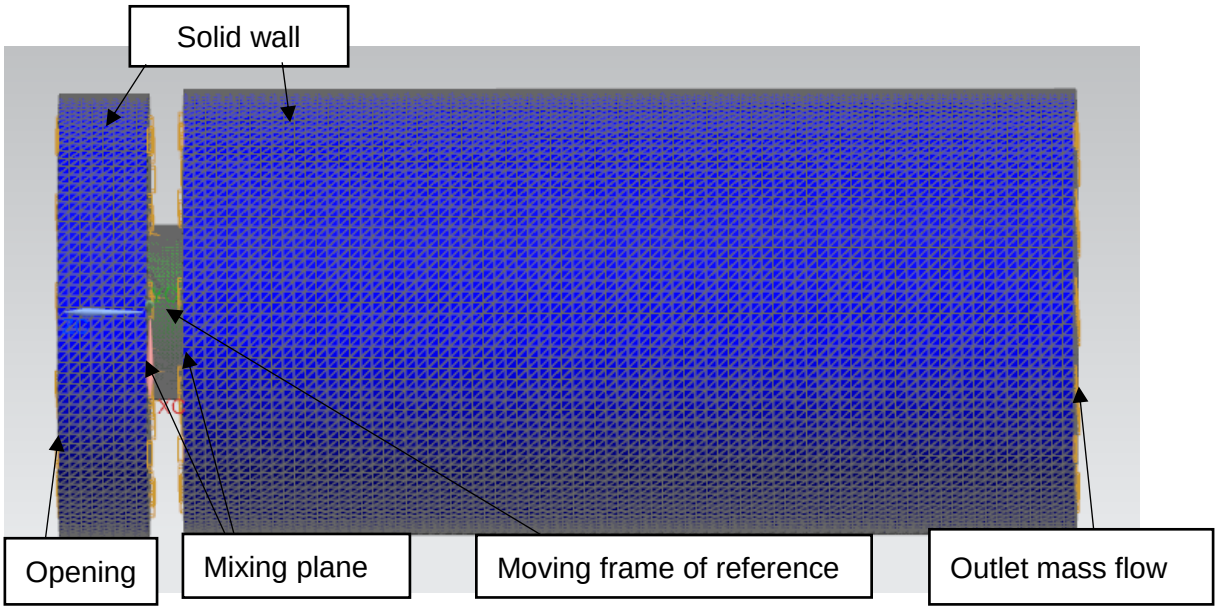

Figure 6.12. Boundary condition.

6.2.6 Solving methods of the steady calculation

At Solver Environment, for solver, NX THERMAL/FLOW and flow analysis type were chosen for the simulation.

The results are obtained with the solution of the continuity, N-S equations along with the equations for the selected turbulence model. The steady simulation is adopted for solution type.

6.2.6.1 Turbulence

In the turbulent regimen, fluctuation occurs at the average speed and its effects should be incorporated in the CFD model to make it consistent. This can be done by using turbulent model. Various methods are available to include turbulent effect in the Navier-Stokes equations and all the methods available have average process over time for the conservation equations.

When the turbulent occurs in the simulation, the velocity is considered to be the sum of an average component and a fluctuation ($U_i + u_i'$). Thus, the average Navier-Stokes equation (RANS, Reynolds-Averaged Navier-Stokes) is:

$$\underbrace{\rho g_i}_{(1)} + \underbrace{F_i}_{(2)} \underbrace{- \frac{\partial p}{\partial x_i}}_{(3)} + \underbrace{\frac{\partial}{\partial x_j}\left[\mu_t\left(\frac{\partial U_i}{\partial x_j} + \frac{\partial U_j}{\partial x_i} - \frac{2}{3}\frac{\partial U_k}{\partial x_k}\delta_{ij}\right)\right] + \frac{\partial}{\partial x_j}(-\rho\overline{u_i' u_j'})}_{(4)} = \underbrace{\frac{\partial(\rho U_i)}{\partial t} + \frac{\partial}{\partial x_j}(\rho U_i U_j)}_{(5)}$$

The different terms correspond to the gravity force (1), external forces applied to the fluid (2), pressure forces (3), viscous forces (4), and inertial forces (5).

The $\overline{u_i' u_j'}$ terms are called Reynold stress and the top bars shows that the terms have average value over time. δ_{ij} is delta tensor, defined as δ_{ij}= 1 for i = j and δ_{ij} = 0 for i≠ j.

The turbulent viscosity, μ_t, is evaluated using turbulence models. The most common one is the k-ε turbulence model (one of many RANS turbulence models). It consists of solving two additional equations for the transport of turbulent kinetic energy, k, and turbulent dissipation, ε.

NX10 software provides various turbulent model that can be used to calculate the simulation depending on which kind of result we need. The available models are [13]:

1. None (Laminar Flow)
2. Fixed Turbulent Viscosity
3. Mixing Length
4. K-Epsilon
5. K-Omega
6. SST — Shear Stress Transport
7. LES — Large Eddy Simulation

K-epsilon was chosen for the turbulence model used in the simulation. It is a standard high-Re model proposed by Launder and Spalding in 1972 [14] and it can calculate recirculation or separation flow. K-epsilon model only need initial or boundary condition for calculation, give a good result and widely acceptable model.

6.2.6.2 Iterations and Residuals

The required number of iterations is determined by setting convergence criteria for the residuals for the three components of velocities, the continuity equation and the variable for the turbulence model [k and ε]. In most cases, the convergence criterion is set such that the difference between two successive iterations [residuals] is five orders of magnitude lower than the initial value.

Therefore, it is not possible to compare simulations whose residuals are 10^{-2} with simulations whose residuals 10^{-3} or 10^{-4}. For the simulation in this project, all the residuals reach at least 10^{-4}.

6.2.7 Comparison of the experimental and numerical results of the axial fan

To validate the simulations, a comparison has to be made between the experimental and numerical results. Average velocity at several points have been taken experimentally by using the anemometer GVA0430 with an accuracy ±2%. The experimental values of average velocity were recorded at Table 4.12. and 4.13.

For the numerical results, average velocity at 5 cm and 30 cm from the axial fan were measured. For 5 cm, average velocity was 2.79 m/s as can be seen from Figure 6.13. The value is almost same with the experimental value which is 2.8 m/s. At 30 cm, the numerical velocity is 0.814 m/s. The value is not very far from the experimental value which is 0.96 m/s.

Average velocity at the inlet of axial fan was measured numerically and the value was 1.729 m/s (Figure 6.14.). The value that was recorded experimentally at inlet was 1.18 m/s. The different in values can be because experimentally, the point where measurement of average velocity taken was 5 cm from the axial fan while in the simulation, the distance only 4 cm.

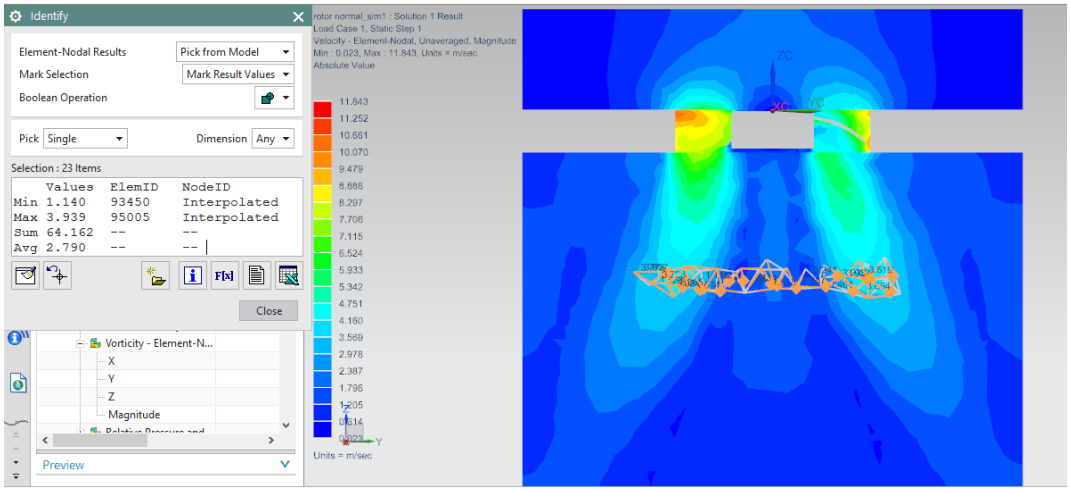

Figure. 6.13. Average velocity value at 5 cm from the axial fan.

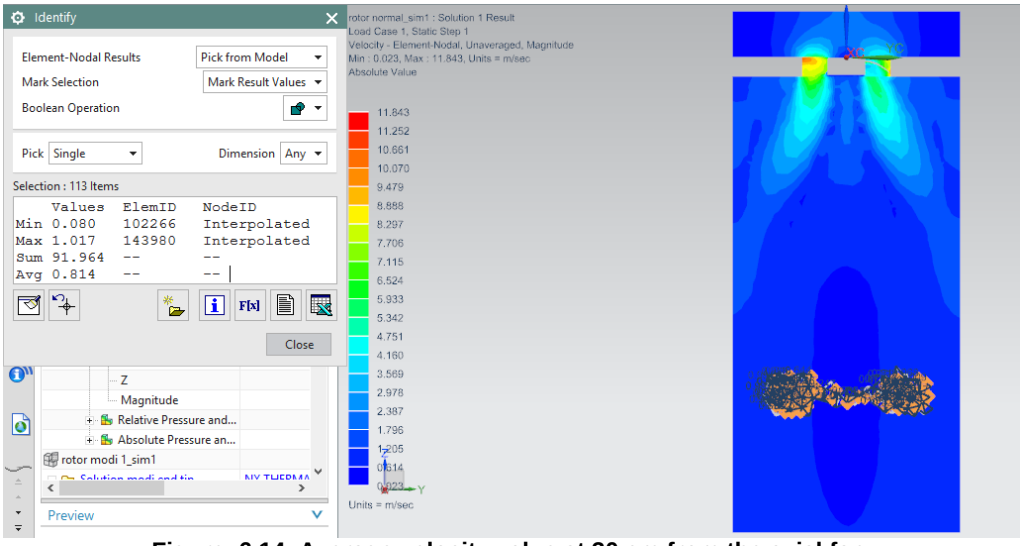

Figure. 6.14. Average velocity value at 30 cm from the axial fan.

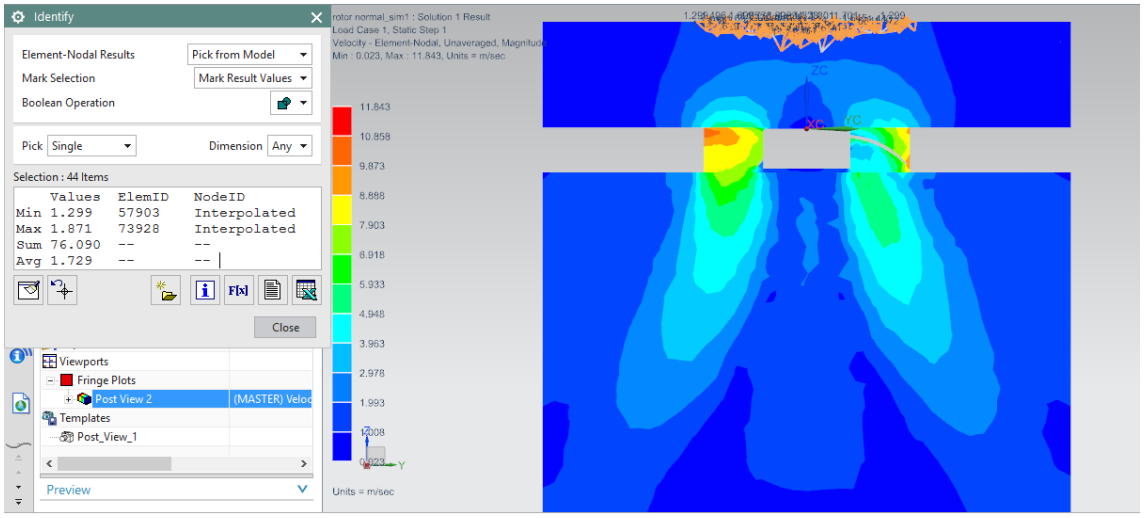

Figure. 6.15. Average velocity value at 5 cm from the axial fan at the inlet.

Values of experimental velocity and numerical velocity at different points were recorded in the table 6.2. and relative error obtained by using:

$$E_{r,ex} = \frac{theoric\ value - experimental\ value}{theoric\ value} \cdot 100$$

Graph of comparison of result between experimental and numerical results was plotted at Figure 6.16 shows

Distance (cm)	Experimental velocity (m/s)	Numerical velocity (m/s)	Relative experimental error (%)
5	2.8 ± 2%	2.79	-0.36
10	2.6 ± 2%	2.017	-28.90
15	1.95 ± 2%	1.293	-50.81
20	1.4 ± 2%	1.166	-20.07
25	1.15 ± 2%	1.083	-6.19
30	0.96 ± 2%	0.814	-17.94

Table 6.2. Experimental and numerical results.

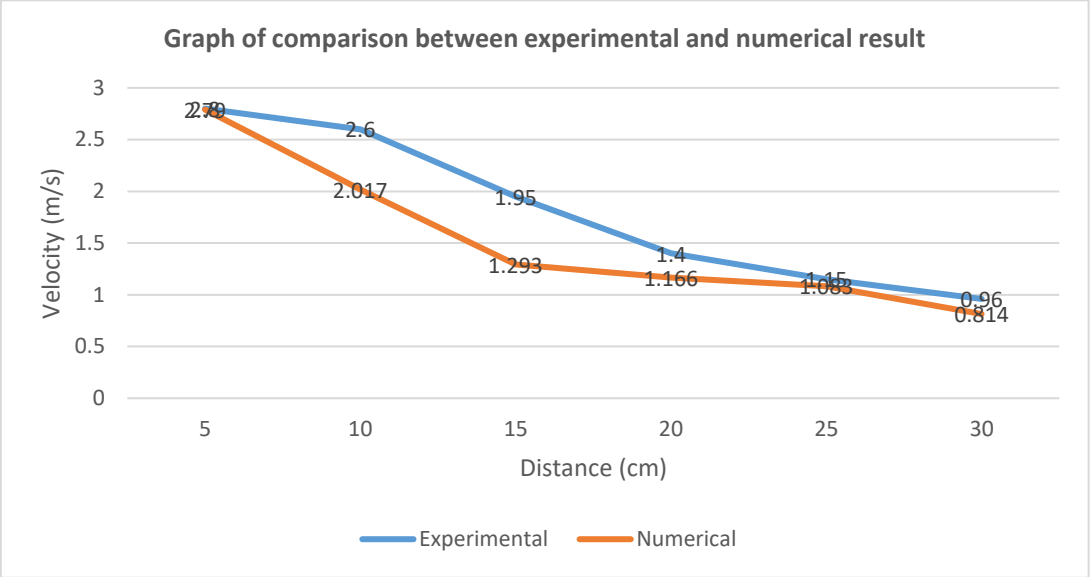

Figure 6.16. Graph of comparison between experimental and numerical results.

Simulation values obtained were inferior to the experimental values showing the great variation within a distance of 15 cm and the error decreasing towards the ends of flow field. There are always exists a discrepancy between experimental measurements and numerical simulation for any engineering problems. It may be due to either simulation error or experimental error or both.

It can be said that the numerical calculation methods are feasible for this project.

6.3 Modification

Based on the prototype which have smooth blade that will be called by model 1, 2 modified models with different parameters of tip end-plate and shark fin blades are established as shown in Fig 6.18. and Fig. 6.19. Model 2 is the geometry of 2 mm width which is in-constant along the chordwise. Model 3 is a geometry of shark fin blade. The spacing between the 3-shark fin blade on the surface of blade is 5 mm.

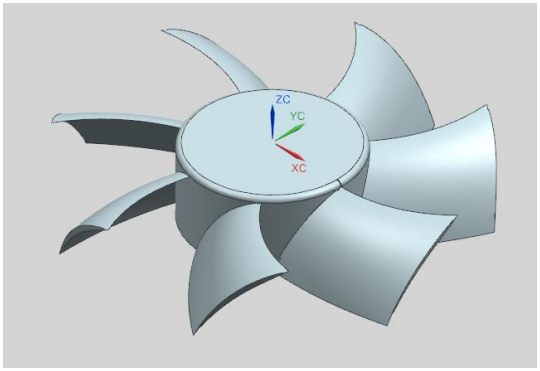

Figure 6.17. Model 1 (Prototype).

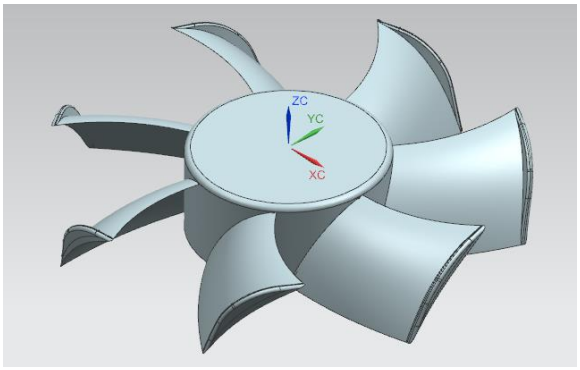

Figure 6.18. Model 2 (Winglet).

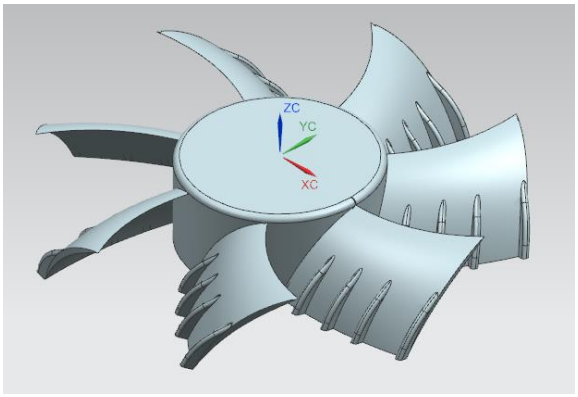

Figure 6.19. Model 3 (Shark fin blade).

6.3.1 Mechanism analysis of the modified models

The internal flow characteristics of a cooling fan are the key factors that affect the static characteristics and aerodynamic performance. Therefore, by analysing the internal flow characteristics of a fan is a feasible method to determine the mechanism of their regular designs. Analysing can be done by observing axial velocity contour of the meridional plane the fans.

Fig. 6.20. shows the axial velocity contours of the meridional plane (X=0) of the airfoils when the rotational velocity is 2000 rpm and the mass flow rate is 0.0242 kg/s. Generally, vortexes were formed at the downstream of the hub at all models and at model 3, the vortexes formed at a middle of downstream were slightly smaller than in the other models.

The formation of vortexes at the upstream and downstream can also be seen clearly at Fig. 6.21. However, there are not much different between the three models.

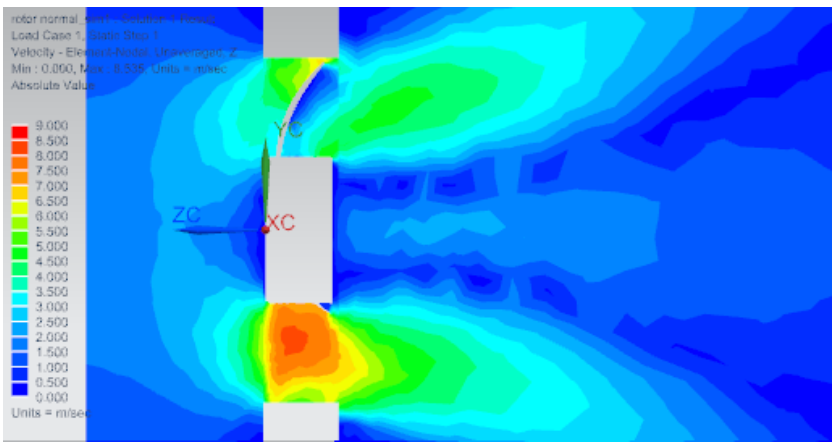

(a) Model 1

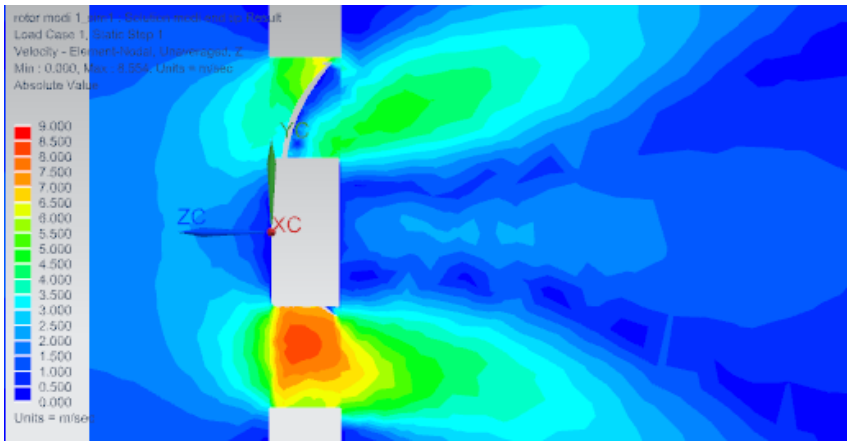

(b) Model 2

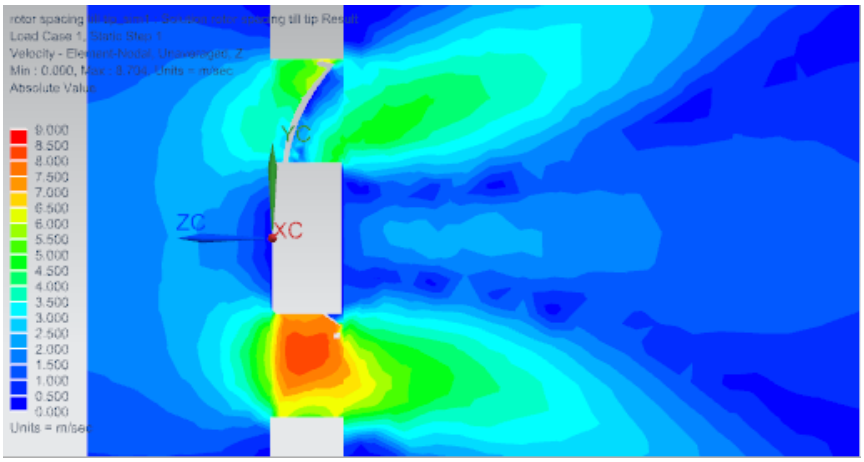

(c) Model 3

Figure 6.20. Axial velocity contours of the meridional plane (X=0).

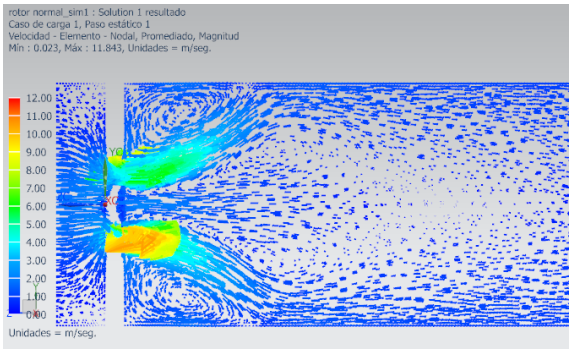

(a) Model 1

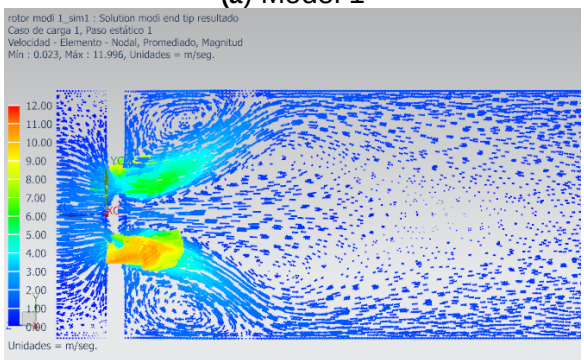

(b) Model 2

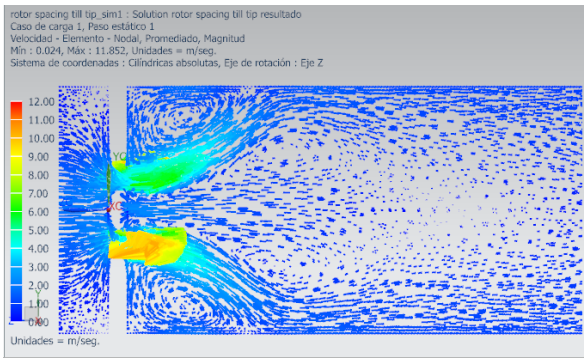

(c) Model 3

Figure 6.21. Axial velocity with arrows of the meridional plane (X=0).

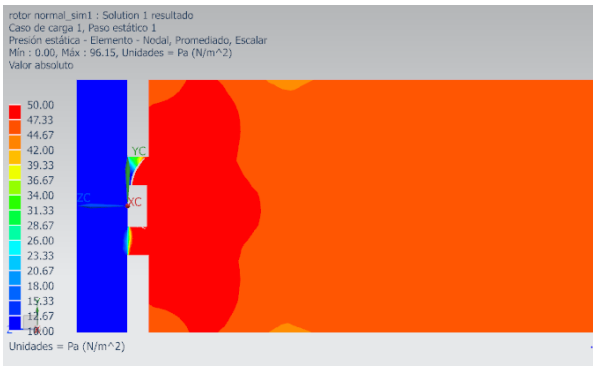

(a) Model 1

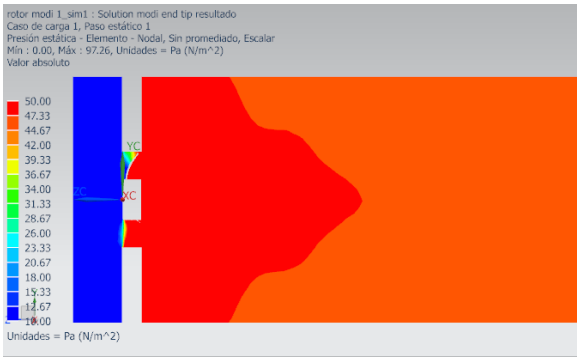

(b) Model 2

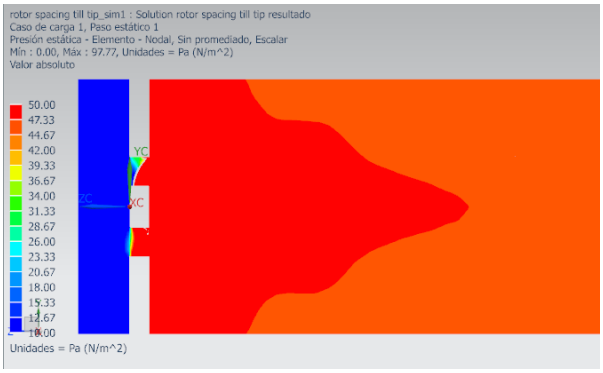

(c) Model 3

Figure 6.22 Static pressure contours of meridional plane (X=0).

It can be seen from the Fig. 6.22 that the static pressure in the model 3 is more concentrated to the middle of plane than model 2.

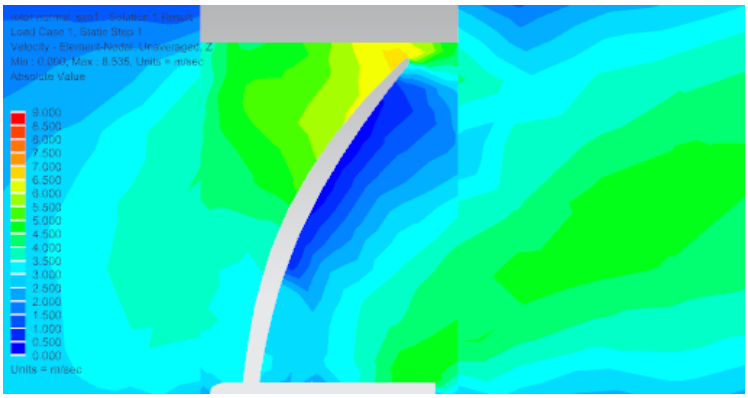

(a) Model 1

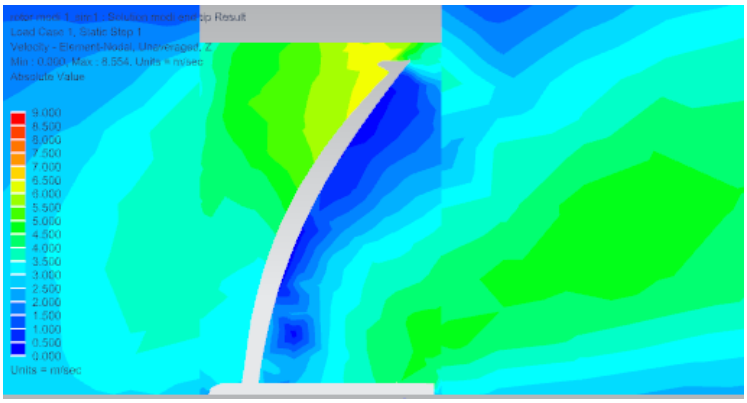

(b) Model 2

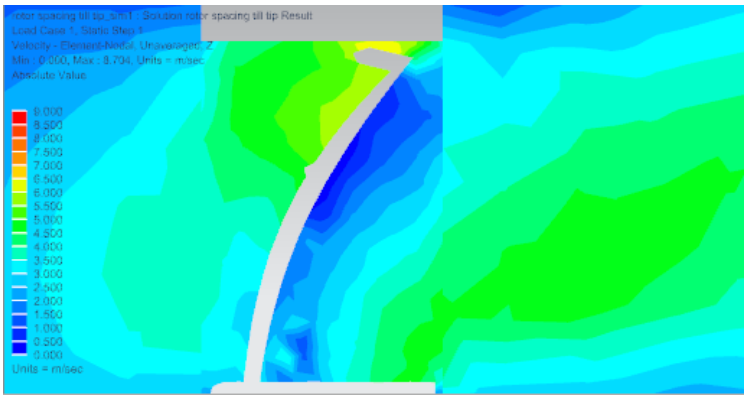

(c) Model 3

Figure 6.23. Detail of axial velocity contours of the meridional plane (X=0).

As we can see, Fig. 6.23, at the tip of blade for model 1, its velocity is higher compare to velocity at the tip for model 2 and 3. Winglet at model 2 and model 3 change the rate of velocity at the tip of blade. It can be seen that vortex mainly occurs at the hub of model 2 and 3.

At model 3, the vortexes were scatter into smaller vortexes. The shark fin blade at the suction side caused more channel turbulence [12]. At model 2, the vortex formed at hub much bigger than at model 3.

Figure 6.24 shows the static pressure contours of the meridional plane for model 1 and model 2. The difference of static pressure between suction surface and pressure surface is shown in the figure by 2 points. The difference of 2 points at model 2 (9.726 Pa) is smaller than model 1 (11.766 Pa), therefore vorticity at the tip of model 2 is smaller [15].

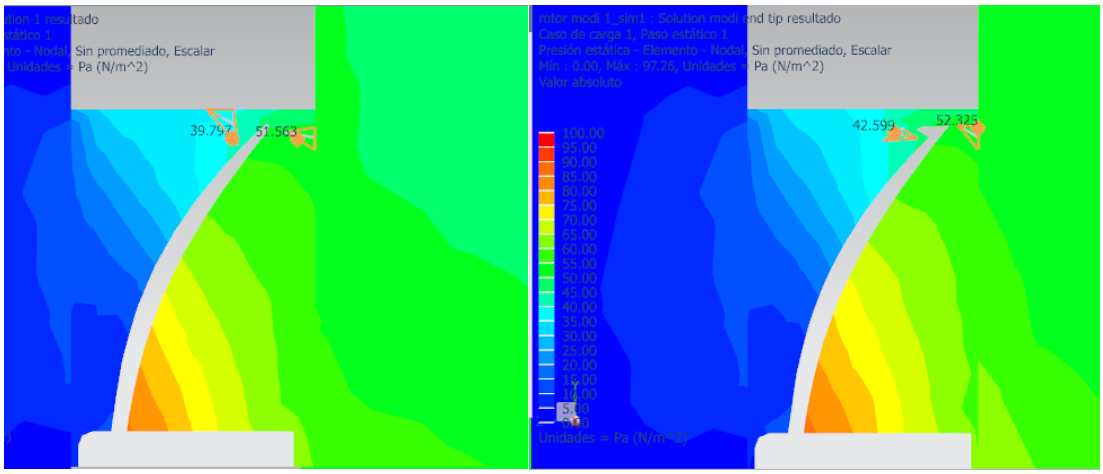

(a) Model 1 (b) Model 2

Figure 6.24. Static pressure contours of the meridional plane (X=0) of the fans.

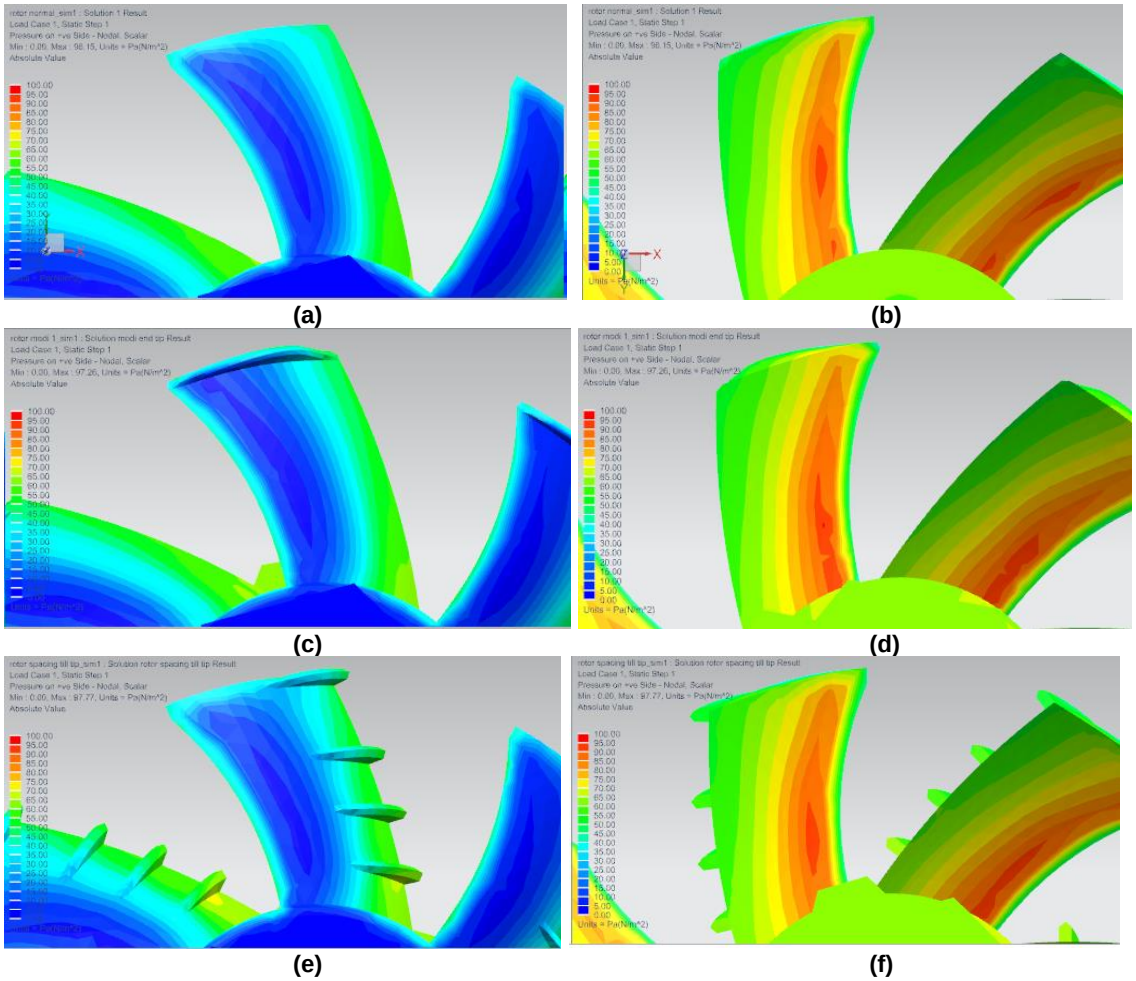

(a) (b)

(c) (d)

(e) (f)

Figure 6.25. Static pressure contours distribution of the blade suction surface and the pressure surface of the three models: (a) Suction surface of model 1; (b) Pressure surface of model 1; (c) Suction surface of model 2; (d) Pressure surface of model 2; (e) Suction surface of model 3; (f) Pressure surface of model 3.

Figure 6.25. shows the contour distribution of static pressure on suction surface and pressure surface for three models of axial fan when the mass flow rate is 0.0242 kg/s. It can be seen that the static pressure of pressure surface is generally higher than that of suction surface. The pressure gradient between the suction surface and the pressure

surface is the key factor that cause leakage around the tip or known as a tip leakage vortex.

Adverse pressure gradient occurred at the suction surface because the airflow passes through side which have less pressure to the side that have higher pressure. This can cause boundary layer separation that will form vortex (wake).

At the pressure surface of the blade, the gradient pressure is favourable to the flow because the airflow passes through higher pressure to less pressure. Therefore, flow separation does not occur.

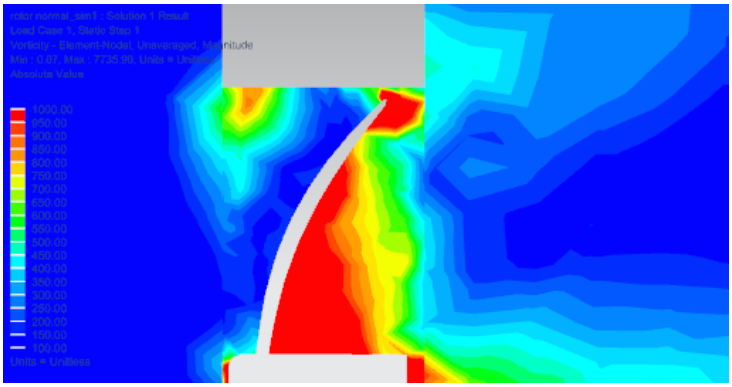

(a) Model 1

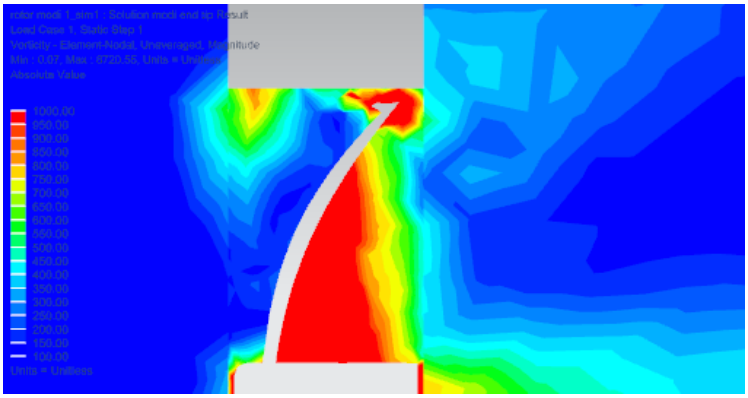

(b) Model 2

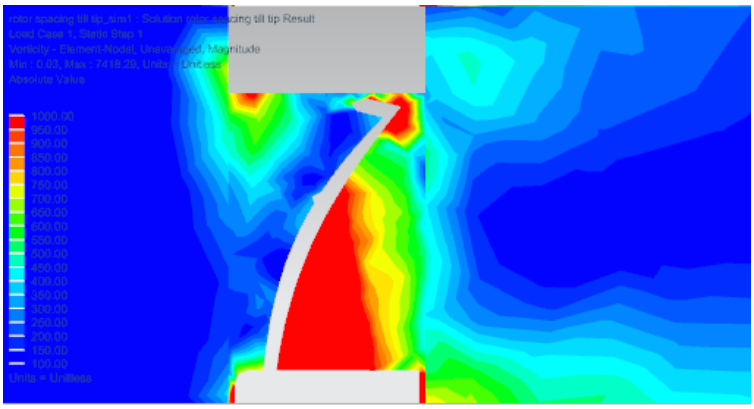

(c) Model 3

Figure 6.26. Vorticity contours distributions of the meridional plane (X=0) of the fans.

Several vortex formations can be seen clearly at Figure 6.26. At model 3, the vortex keeps changing at the suction surface. The shark fin blade caused the smaller vortex occurs at the pressure surface. This phenomenon can be see clearly at Figure 5.3. It advantage is to increase the airflow [12].

At the tip of blade of model 1 and 3, the vortex formed at tip of the pressure side of blade while for model 2, the vortex formed around the tip of blade. At the downstream, the big vortex was scatter to smaller vortexes at model 2 while at model 3 the vortex was slightly bigger than at model 1. The vortex that form near the hub for model 3 is little bit smaller than the other models.

In order to further study the internal flow characteristics about fan, velocity distribution was analysed. Fluid flow was observed from three different axial cross-sections, which are cross-sectional Z = -2 mm (inlet of passage), Z = -7,5 mm (intermediate of passage), Z = -13mm (outlet of passage) (Figure 6.27).

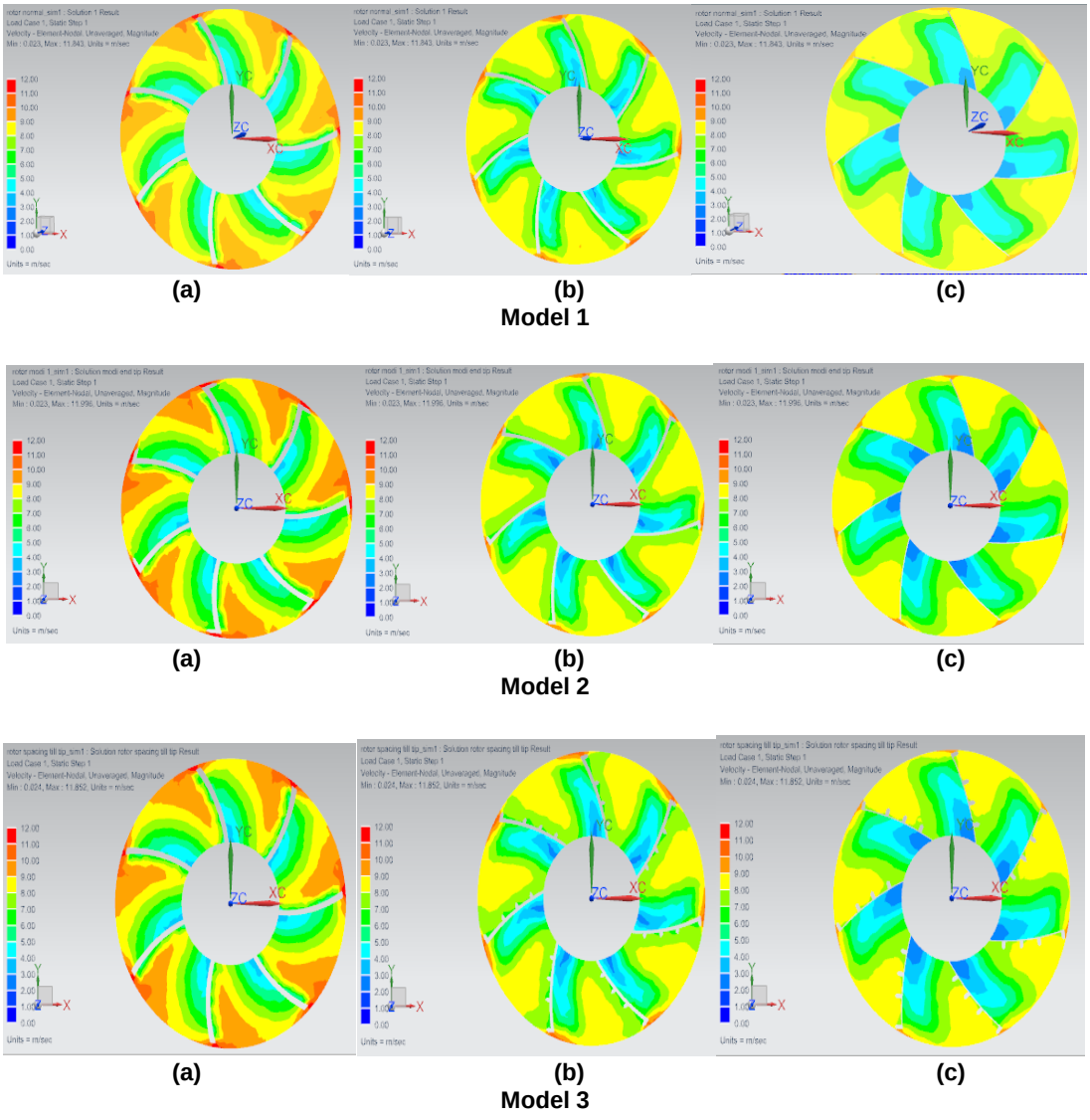

Figure 6.27. Three different axial cross-sections, which are cross-sectional a:(inlet of passage), b: (intermediate of passage), c: (outlet of passage).

Figure 6.27 shows the speed of airflow when it enter the rotating body. Generally, speed of airfow is the highest at the tip of blade. Airflow is very fast when it enter the passage then it velocity decrease gradually until it pass through the outlet passage. The airflow at the outlet of passage is more stable where the velocity is mainly between 9 m/s to 4 m/s.

The differences of velocity at different passage can be caused by the diffuser effect, by increasing the passage section through the blades (Fig. 6.28). Diffuser effect can reduce average velocity of flow and increase it average pressure. This will lead to boundary layer separation due to adverse pressure gradient.

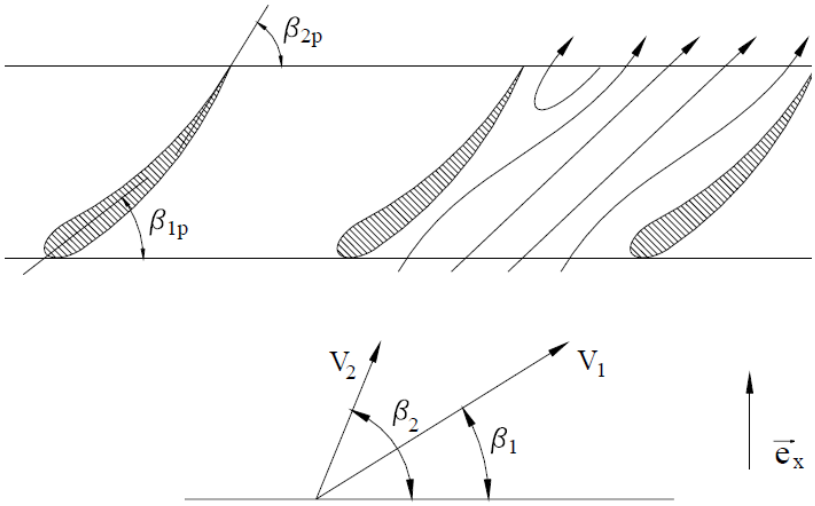

Figure 6.28. Diffuser effect [16].

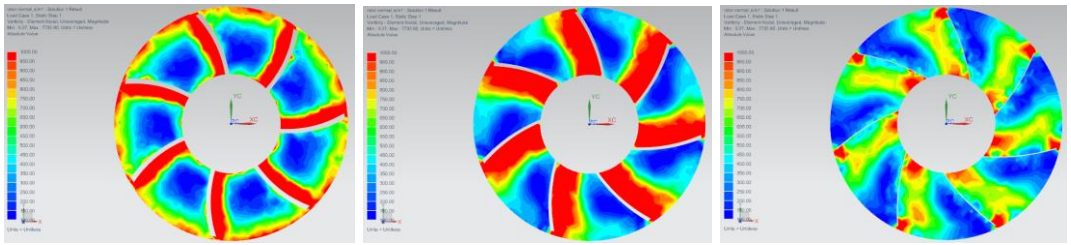

(a) (b) (c)
Model 1

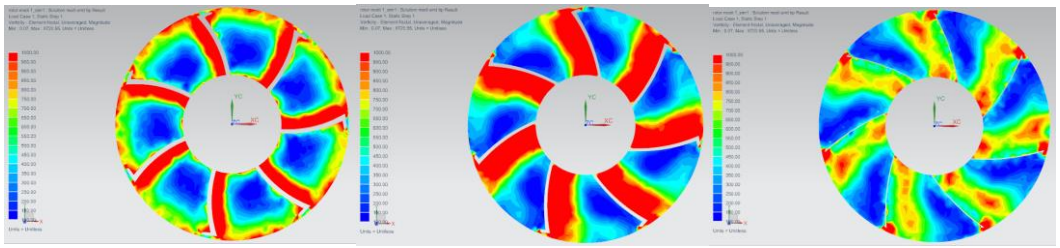

(a) (b) (c)
Model 2

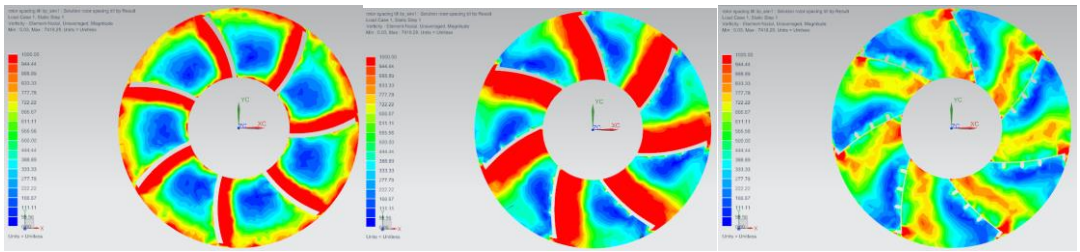

(a) (b) (c)
Model 3

Figure 6.29. Three different cross-sections of vorticity, which are cross-sectional a:(inlet of passage), b: (intermediate of passage), c: (outlet of passage).

Figure 6.29 shows the vorticity in three sections of different models. It can be observed that the vorticity at model 3 is generally smaller than the other models.

The formation of vortexes for model 1, Fig. 6.29 (c), occurred clearly at tip of blade and near the hub. For model 2, the vortexes at the outlet passage occurred mostly near to the winglet and at the hub, but the vortexes are located in a larger area of the passage. It can be seen clearly that at model 3(c) the vortex occurs in the space between the suction surface and the pressure surface along the way from hub to the winglet. Near the hub, vortex intensity at model 1 is slightly bigger than the other models.

7. Conclusion

The project introduced 2 modifications on small axial fan which are winglet (model 2) and shark fin blades (model 3). With the help of numerical simulation and experimental testing, the effect of modifications that have been made on the aerodynamic performance, static pressure characteristic and the internal flow field were determined. The mechanism analysis of the modified models was discussed. The conclusions are summarized as follows:

1) The difference between the models 1 and 2 shown that the presence of a winglet reduces the vortices created by the reduction of differential pressure between the pressure surface and suction surface at the tip of blade.

2) Diffuser effect can reduce average velocity of flow and increase it average pressure. This will lead to boundary layer separation due to adverse pressure gradient.

3) Vortexes formed at downstream at model 2 were much smaller. In model 3 (shark fin blade), the vorticity near the hub was smaller than the other models.

4) Vortexes were more concentrated at the tip of blade and near hub for model 1 but it was different for model 2 and 3. The vortexes occurred along the blade between the passage from hub to tip of blade.

5) Adding shark fin blade at the suction surface of blade can help to channel the turbulence therefore reduce the vortex effect near the hub and at trailing edge of blade.

The decreasing vorticity that have been observed in the flow of model 2 and model 3 can be relate with a possibility of noise reduction for axial fan as have been told by the manufacturer [12] and the authors [2],[15].

8. Recommendations

There are few recommendations for further work to overcome the problems and to improve the results in this project which are:

1. Fabricate a solid axial fan for model 2 and 3. Then do an experiment to see the overall characteristic and compare the experimental results with numerical solution.

2. Perform an experiment for noise testing for all model by using international standard ISO10302, which is a standard method for measuring the noise emission of small fan. This can help to make a comparison between experimental measurements and numerical simulation.

9. Acknowledgement

I would like to express my deepest appreciation to Monserrat Carbonell Ventura, my project's supervisor and mentor. She has been very supportive, helpful and also her kindness to help and guide me to coordinate and finish this project on time.

I would like to acknowledge with much appreciation to the technical staff, Oscar De Sousa. Without all their help, this project wouldn't be finished. Not to forget, my family and friends who always support me from behind to finish my degree here at EPSEVG. It has been a very wonderful journey.

10. References

[1] A. Corsini, A. G. Sheard, “Tip End-Plate Concept Based On Leakage Vortex Rotation Number Control,” Journal of Computational and Applied Mechanics, Vol 8., No. 1, pp.21-37, 2007.

[2] H. Mao, Y. Wang, P. Lin, Y. Jin, S. Tosh, and K. D. Heuy, “Influence of Tip End-plate on Noise of Small Axial Fan,” *J. Therm. Sci.*, vol. 26, no. 1, pp. 30–37, 2017.

[3] L. Zhang, Y. Jin, and Y. Jin, “An investigation on the effects of irregular airfoils on the aerodynamic performance of small axial flow fans,” *J. Mech. Sci. Technol.*, vol. 27, no. 6, pp. 1677–1685, 2013.

[4] L. Zhang, Y. Jin, and Y. Jin, “Effect of tip flange on tip leakage flow of small axial flow fans,” *J. Therm. Sci.*, vol. 23, no. 1, pp. 45–52, 2014.

[5] C. Arce León, D. Ragni, S. Pröbsting, F. Scarano, and J. Madsen, “Flow topology and acoustic emissions of trailing edge serrations at incidence,” *Exp. Fluids*, vol. 57, no. 5, p. 91, 2016.

[6] L. Zhu, Y. Jin, Y. Li, Y. Jin, Y. Wang, and L. Zhang, “Numerical and experimental study on aerodynamic performance of small axial flow fan with splitter blades,” *J. Therm. Sci.*, vol. 22, no. 4, pp. 333–339, 2013.

[7] Roque, "Triângulos De Velocidade", Universidade Federa do Paraná.

[8] W. W. Peng, *Fundamentals of Turbomachinery*. New Jersey, USA: Ed. John Wiley & Sons, 2008, pp 369.

[9] L. Patiño and M. Solano, "Máquinas Hidráulicas", Editorial U.P.V, Universitat Politècnica de Valencia, 1999.

[10] LYF 4pin 12V 8cm 8015s 80mm x 15mm DC Brushless PC CPU Lüfter cooling cooler fan. [Online]. Available: http://www.ebay.com/itm/LYF-4pin-12V-8cm-8015s-80mm-x-15mm-DC-Brushless-PC-CPU-Lufter-cooling-cooler-fan-/262599253953?hash=item3d24229fc1

[11] WING 9 UV BLUE [Online]. Available:http://gelidsolutions.com/thermal-solutions/wing-9-uv-blue/

[12] ZM-SF2 Shark’s Fin Blade 92mm Silent Fan. [Online]. Available: http://www.zalman.com/contents/products/view.html?no=351

[13] Understanding the turbulence models. [Online]. Available: https://docs.plm.automation.siemens.com/tdoc/nx/10/nx_help#uid:id629636

[14] P. Goncharov, I. Artamonov and T. Khalitov, Engineering Analysis with NX Advanced Simulation. Siemens Product Lifecycle Management Software Inc. 2014.

[15] S. A. Beskales, Samir S. Ayad, M. G. Higazy and O. E. Abdellatif, " The Effect of Tip End-blade Geometry on the Axial Fans Performance," presented at Eleventh International Conference of Fluid Dynamics, Alexandria, Egypt, 2013

[16] "Máquinas Axiales," Maquinas Para Fluidos 1, Instituto de Mecánica de Los Fluidos e Ingeniería Ambiental. [Online]. Available: https://www.fing.edu.uy/imfia/cursos/maq_flu_1/teorico/7-Axiales.2009.pdf

[17] Bhaskar Roy and A. M. Praadeep “Turbomachinery Aerodynamics” Lect-8, Department of Aerospace Engineering, IIT Bombay. [Online]. Available: http://nptel.ac.in/courses/101101058/downloads/Lec-08ppts.pdf

[18] C. Willimas, Fans & Ventilation, A Practical Guide, Elsevier Science, 2005.

[19] R. A. Wallis, Axial Flow Fans, Design and Practice. New York 3, New York: Academic Press, 1961.

[20] E. Dick, “Fans,” in *Fundamentals of Turbomachines*, Dordrecht: Springer Netherlands, 2015, pp. 97–151.

[21] M. T. Schobeiri, “Introduction, Turbomachinery, Applications, Types,” in *Turbomachinery Flow Physics and Dynamic Performance*, Berlin, Heidelberg: Springer Berlin Heidelberg, 2012.

[22] M. T. Schobeiri, “Basic Physics of Laminar-Turbulent Transition,” in *Turbomachinery Flow Physics and Dynamic Performance*, Berlin, Heidelberg: Springer Berlin Heidelberg, 2012, pp. 515–544.

[23] Siemens Documentation: NX 10.0.3 Help. [Online]. Available: https://docs.plm.automation.siemens.com/tdoc/nx/10.0.3/nx_help/#uid:index

[24] Vane Axial, Application and Design, GREENHECK. [Online]. Available: http://www.greenheck.com/media/pdf/otherinfo/VaneAxial_Application_Perf_Supplement.pdf

[25] W. Terry, Fluid Machinery: Performance, Analysis, and Design. Boca Raton, Florida, United States: CRC Press, 1999.

[26] L. Zhang, Y. Jin, D. Hua and Y. Jin, “Numerical and experimental investigation on aerodynamic performance of small axial flow fan with hollow blade root,” *J. Therm. Sci.*, vol. 22, no. 5, pp. 424–432, 2013.

[27] C. Huang and C. Gau, “An optimal design for axial-flow fan blade: theoretical and experimental studies,” *J. Mech. Sci. Technol.*, vol. 26, no. 2, pp. 427–436, 2012.

[28] S. L. Dixon, Fluid Mechanics and Thermodynamics of Turbomachinery, United States of America: Butterworth Heinemann, 1998.